



REPUBLIC OF IRAQ

MINISTRY OF HIGHER EDUCATION AND

SCIENTIFIC RESEARCH

AL-FURAT AL-AWSAT TECHNICAL UNIVERSITY

ENGINEERING TECHNICAL COLLEGE- NAJAF

DESIGN AND SIMULATION AN ABSORBER BASED

ON FRACTAL GEOMETRY IN X- BAND APPLICATIONS

WASSAN HASSAN YASEEN

(M. Sc. Communication Techniques Eng.)

2022



**DESIGN AND SIMULATION AN ABSORBER BASED ON FRACTAL
GEOMETRY IN X- BAND APPLICATIONS**

**THESIS SUBMITTED TO COMMUNICATION TECHNIQUES
ENGINEERING DEPARTMENT IN PARTIAL FULFILLMENT OF
THE REQUIREMENTS FOR THE TECHNICAL MASTER DEGREE
IN**

COMMUNICATION ENGINEERING

BY

Wassan Hassan Yaseen

Supervised by

Prof.Dr Abdulkadhum Jafar Alyasiri

Dr. Ghufran Mahdi Hatim

October/2022

SUPERVISORS CERTIFICATION

We certify that the thesis entitled “**Design and Simulation an Absorber Based on Fractal Geometry in X- Band Applications**” which is being submitted by **Wassan Hassan Yaseen** was prepared under our supervision at the Communication Techniques Engineering Department, Engineering Technical College – Najaf, AL. Furat Al - Awsat Technical University, as partial fulfillment of the requirements for the degree of Master of Communication Techniques of Engineering.

Signature:

(Supervisor) **Prof. Dr. Abdulkadum Jafar Alyasiri**

Date: / /2022

Signature:

(Co-supervisor) **Dr. Ghufraan Mahdi Hatim**

Date: / /2022

In view of the available recommendation. We forward this thesis for debate by the examining committee.

Signature:

Name: **Prof. Dr. Ahmed T. Abdulsadda**

Head of Communication Tech. Eng. Dept.

Date: / /2022

COMMITTEE REPORT

This Thesis [**Design and Simulation an Absorber Material Based on Fractal Geometry in X- Band Applications**] which is being submitted by **Wassan Hassan Yaseen** and as examining Committee, examined the student in its contents. In our opinion, the thesis is adequate for award of degree of Master.

Signature:

Name: **Prof. Dr. Abdulkadum Jafar Alyasiri**
(Supervisor)

Date: / / 2022

Signature:

Name: **Dr. Ghufran Mahdi Hatim**
(Co-supervisor)

Date: / / 2022

Signature:

Name: **Dr. Mohanad Ahmed Al-Ibadi**
(Member)

Date: / / 2022

Signature:

Name: **Asst. Prof. Dr. Ahmed Obaid Aftan**
(Member)

Date: / / 2022

Signature:

Name: **Prof. Dr. Thamir R. Saeed**
(Chairman)

Date: / / 2022

Approval of the Engineering Technical College- Najaf

Signature:

Name: **Asst. Prof. Dr. Hassanain Ghani Hameed**
Dean of Engineering Technical College- Najaf

Date: / / 2022

LINGUISTIC CERTIFICATION

This is to certify that this thesis entitled “**Design and Simulation an Absorber Based on Fractal Geometry in X-Band Applications**” was reviewed linguistically. Its language was amended to meet the style of the English language.

Signature:

Name:

Date:

ABSTRACT

Absorbing the electromagnetic signals reflected from the aircraft is a crucial topic in military applications. Reducing the power amount of the reflected waves plays a vital role in determining the aircraft's location in the sky. This thesis will deal with this issue by introducing a new synthesized absorptive material SAM. The proposed SAMs can reduce the reflection power by more than 95%, and this reduction will provide a good alternative for military and commercial applications.

Three different unit cells based on the fractal geometry are proposed. The proposed unit cells are arranged in planes to create the Left-handed materials LHMs (i.e., SAM), which can confine the incident power instead of returning it to from where they come because the SAM has negative permittivity and permeability at specific ranges of the frequencies, operating at the X-band (8-12GHz). All designs and simulations adopt the FR4 substrate with a dielectric constant of 4.3, a thickness of 1mm, and a loss tangent of 0.025. The proposed unit cells are printed on the top copper face of the substrate.

The Apollonian Gasket fractal geometry is the first simulated unit cell type. There is an air gap between the absorber slots. The results show that the structure has the highest absorption ratio of 99.7% observed at 10 GHz with a 1.5 GHz bandwidth. Due to changes in the equivalent relative permeability and permittivity of the structure, the overall absorber performance has been enhanced. The second designed structure is based on the modified ring sun fractal geometry where the unit cell is cut out of the absorber patch. The results show that the design has the maximum absorption of 95.5% at 8.9 GHz with a 1.3 GHz bandwidth. Both absorbers can achieve high absorption in various frequency X-band ranges that might be used in multiple military radar applications. The design structures are studied and simulated using the CST microwave studio package. Finally, the thesis introduces another type of SAM with a high absorption ratio.

ACKNOWLEDGMENTS

In the name of **ALLAH**, the **Most Gracious** and the **Most Merciful**, for giving me the determination and will to complete this research work.

I appreciate the inspiration and guidelines from my supervisors, Prof. Dr. Abdulkadum J. Aliasiri and Dr. Ghufran Mahdi Hatim, for their advice.

I sincerely thank Dr. Nasr Nomas Al-Khafaji for helping me with valuable scientific information, guidance and encouragement, without his continuous support and interest, this work would not have been the same as presented here.

I also want to express my deep gratitude to my best friend, Eng. Dr. Rua'a Shallal Abbas, thank her for standing with me in difficult moments, supporting and encouraging me, always believing in me, and knowing I can achieve my dream.

I want to express my heartfelt thanks to my husband, Eng. Salam Hassan, for unconditional support and encouragement to pursue my interests, for listening to my complaints and frustrations, and for believing in me, I would like to express my thanks to my **family** (My mother, my sisters, and my brothers).

Finally but not slightest, my female friends and my colleagues, special mention: Eng. Miss. Noor Fadhel, Eng. Dr. Quhtan Mutar, Eng. Bahaa Hamzah Jasim, and Eng. Ahmad Alaa, for their help and wishes for the successful completion of this project and for supporting me during the study period

DECLARATION

I hereby declare that the work in this thesis is my own except for summaries that have been duly acknowledged.

Date: / / 2022

Wassan Hassan Yaseen

TABLE OF CONTENTS

SUPERVISORS CERTIFICATION	iv
COMMITTEE REPORT	v
LINGUISTIC CERTIFICATION	vi
ABSTRACT.....	viii
ACKNOWLEDGMENT	xi
DECLARATION	xii
CONTENTS.....	xv
LIST OF TABLES	
LIST OF FIGURES.....	
LIST OF ABBREVIATIONS.....	
CHAPTER ONE	1
1.1 INTRODUCTION.....	1
1.2 Literature Review	6
1.3 Problem Statement.....	16
1.4 Scope and Motivation of the Project	17
1.5 Aim of the Work.....	17
1.6 Research Contribution	17

1.7 Thesis Layout	18
CHAPTER TWO	19
THEORETICAL BACKGROUND	19
2.1 Theoretical analysis	19
2.2 Metasurface	21
2.3 Geometry of Fractals	25
2.4 Negative Refractive Index	27
2.5 Feeding Techniques	30
2.6 Waveguide feed	30
2.7 Extraction of Metasurface Parameters	31
2.7.1 Method Definition	31
2.7.2 Mathematical Formulation	32
2.7.3 Simulation and Extraction of Results	35
2.8 Apollonian	36
CHAPTER THREE	39
DESIGN CONFIGURATION	39
3.1 Introduction	39
3.2 Research Methodology	39
3.3 The Proposed Model (I): Apollonian	41
3.4 The Proposed Model (II): Modify for Apollonian	42

3.5 The Proposed Model (III): Design of Absorber the Sun Fractal Structure.....	45
CHAPTER FOUR.....	47
RESULTS AND DISCUSSION	47
4.1 Introduction.....	47
4.2 Study for Apollonian Gasket Unit Cell Metasurface Absorber(I)	48
4.2.1 Extracting S-Parameter for Apollonian Gasket Fractal Unit Cell Metasurface Absorber	49
4.2.2 Extracting Permeability and Permittivity from S-Parameter	51
4.2.3 Extracting Absorption value from S-Parameters.....	53
4.2.4 Extracting the Refractive Index value from S-Parameters	53
4.2.5 The Current Distribution.....	54
4.3 Study of the 3rd-iteration Modified Apollonian Gasket Unit Cell Metasurface of the Absorber (II).....	55
4.3.1 Extracting S-Parameters, Permittivity, and Permeability of the 3rd-Iteration Modified Apollonian Gasket Metasurface Unit Cell of the Absorber	57
4.3.2 Extracting Absorption Coefficient from S-Parameters.....	59
4.3.3 The Current Distribution.....	59
4.4 Parametric Study of the Sun Fractal Metasurface Absorber Unit Cell	60
4.4.1 Extracting S-Parameter for sun fractal Unit Cell Metasurface Absorber	61
4.4.2 Extracting Permeability and Permittivity from S-Parameter	63

4.4.3 Extracting Absorption value from S-Parameters.....	64
4.4.4 The Current Distribution.....	65
4.5 Comparison and Discussion of the Results.....	66
CHAPTER FIVE.....	71
CONCLUSION AND FUTURE WORK.....	71
5.1 Introduction.....	71
5.2 Conclusions.....	71
5.3 Future Work Recommendations.....	72
REFERENCE:.....	73
APPENDIXES/ PUBLICATIONS	80
Abstract in Arabic	

LIST OF TABLES

CHAPTER ONE

TABLE 1.1: References fractal absorber designs associated with metamaterial	12
---	----

CHAPTER THREE

TABLE 3.1: Design parameters of the proposed Apollonian gasket fractal Metasurface Absorber unit cell	42
--	----

TABLE 3.2: Design parameters of the proposed Apollonian Gasket fractal Metasurface Absorber unit cell	45
--	----

TABLE 3.3: The proposed Sun Fractal Metamaterial Absorber unit cell design parameters	46
--	----

CHAPTER FOUR

TABLE 4.1 Comparisons among the three designs of the proposed absorbers and with other related works.....	70
--	----

LIST OF FIGURES

CHAPTER ONE

Figure 1.1: Radar Pulse Principle [2]	2
---	---

Figure 1.2: Microwave absorbers are used to minimize EMI [3]	3
--	---

Figure 1.3: Microwave absorbers in military applications [4].....	4
---	---

CHAPTER TWO

Figure 2.1: Electric – magnetic- surface wave and Poynting vectors of an electromagnetic wave in RH and LH mediums [24].....	22
Figure 2.2: Collection of thin wires and SRR to shape DNG MTM [24]	23
Figure 2.3: The four possible types of materials based on permittivity and permeability signs [39].....	24
Figure 2.4: Mathematical fractal geometry examples, (a) Sierpinski Gasket, (b) Sierpinski Carpet, (c) Koch Curve, (d) Minkowski (MSK) curve [44]	27
Figure 2.5: Material classification [46]. The angular frequencies: ω_{pe} and ω_{pm} : represent the electric and magnetic plasma frequencies, respectively. R, purely natural. I, strictly imaginary	28
Figure 2.6: (a) Media with right-handed properties (b) Media with Left-handed properties [46].....	29
Figure 2.7: Waveguide feed.....	30
Figure 2.8: Unit cell between two waveguide ports.....	36
Figure 2.9: Different shapes for an Apollonian Gasket [57]	37
Figure 2.10: Structure of the proposed material fractal absorber	38

CHAPTER THREE

Figure 3.1: Shows the Flowchart of the Methodology of the Proposed Absorber	40
Figure 3.2: Proposed absorber structure.....	41
Figure 3.3: Proposed absorber structure.....	43
Figure 3.4: Different iteration stages of Apollonian Gasket fractal structure of the proposed fractal absorber	43
Figure 3.5: Waveguide feed of Apollonian Gasket fractal structure of the proposed fractal absorber.....	44
Figure 3.6: Sun fractal absorber metasurface structure proposed.....	46

CHAPTER FOUR

Figure 4.1: Parametric study of the Apollonian Gasket Fractal Unit Cell	49
Figure 4.2: The S-parameters (S11)	50
Figure 4.3: (A) the permittivity (B) the permeability of metamaterial	52
Figure 4.4: The Absorption value	53
Figure 4.5: the negative refractive index	54
Figure 4.6: current distribution at the resonance frequency	55
Figure 4.7: S11 vs the substrate thickness for the third iteration modified apollonian gasket unit cell metasurface of the absorber.....	56

Figure 4.8: (A) the 3 rd -iteration of Modified Apollonian Gasket metasurface unit cell (B) S11- parameter (C) permittivity (D) permeability	58
Figure 4.9: Absorption value of the 3 rd iteration.....	59
Figure 4.10: Current distributions of the 3 rd iteration	60
Figure 4.11: Parametric study of the Sun fractal metasurface absorber unit cell	61
Figure 4.12: (A) S11 and (B) refractive index (n)	62
Figure 4.13: (A) permittivity (B) permeability values	64
Figure 4.14: AbsorFigure 4.10: Current distributions of the 3 rd iteration	65
Figure 4.15: current distribution for the sun fractal unit cell.....	66
Figure4.16: Comparison of the absorption coefficient of all proposed absorbers	68
Figure 4.17: Comparison of the S11 coefficient of all proposed absorbers	69

LIST OF ABBREVIATIONS

Abbreviations	Description
<i>BW</i>	Bandwidth
<i>CW</i>	Continuous Wave radar
dB	Decibel
<i>EM</i>	Electromagnetic
<i>EMI</i>	Electromagnetic Wave Interference
<i>FR4</i>	A type of Substrate used in designing Absorbers with relative permittivity “ $\epsilon = 4.3$ ” and a loss tangent of 0.025
<i>FSM</i>	Fractal Shaped Metamaterial
<i>LHM</i>	Left-Hand Medium
<i>MTM</i>	Metamaterial
<i>MW</i>	Microwave
<i>PEC</i>	Perfect Electric Conductor
<i>PR</i>	Pulsed Radar
<i>RAM</i>	Radar Absorber Material
<i>RCS</i>	Radar Cross Section
<i>RHM</i>	Right-Hand Medium
<i>SAM</i>	Synthesized Absorbing Material

LIST OF SYMBOLS

Symbol	Definition
$3D$	Three Dimensions
ϵ	Dielectric constant (Permittivity)
ϵ_r	Relative dielectric constant
μ_r	Relative Permeability
ϵ_0	The Permittivity of Free Space
μ_0	The Permeability of Free Space
Δ	Tangent Loss
B	Unit Cell Size
θ	Theta
Φ	Phi
λ_0	Free Space Wavelength
λ_g	Guided Wavelength
N	Refractive Index
ω_{pe}	Electric Plasma Frequencies
ω_{pm}	Magnetic Plasma Frequencies
S_{11}	Reflection coefficient at port 1
S_{12}	Isolation coefficient
S_{21}	Transmission coefficient
Z	Wave Impedance
E	Electric Field Components
H	Magnetic Field Components
$(-)^{\prime\prime}$	Complex Component
$(-)^{\prime}$	Real Component

CHAPTER ONE
GENERAL INTRODUCTION AND
LITERATURE REVIEW

1.1 Introduction

A radar, called “radio detection and ranging,” is an object detection system [1]. A radar is a device for discovering and assessing or calculating a distant objective's location and/or velocity by transmitting a radio frequency signal and receiving returns from the objects (goals) with which they intersect. This returned energy is then processed to read out target data like distance, angular position, velocity, and other targets' comparable features by the radar receiver [2]. Fig. 1.1 shows the basic block diagram of radar [2]. The radar can be categorized into ground, marine, airborne, and spaceborne. It can also be sorted into groups according to their features, such as the frequency band, antenna kind, and waveforms used. Based on the radar function, the radar is classified into weather, acquisition and search, tracking, track-while-scan, fire control, early warning, over the horizon, terrain following, terrain avoidance radars, and military radars. The most common Radar classifications are Continuous Wave radar (CW) and Pulse Radar based on the waveform status. In Continuous Wave radar, electromagnetic energy is transmitted continuously with remote and receiver antennas; in Pulsed radar (PR), the electromagnetic energy is sent as a string of modulated pulses with a standard antenna for transmission and reception [2]

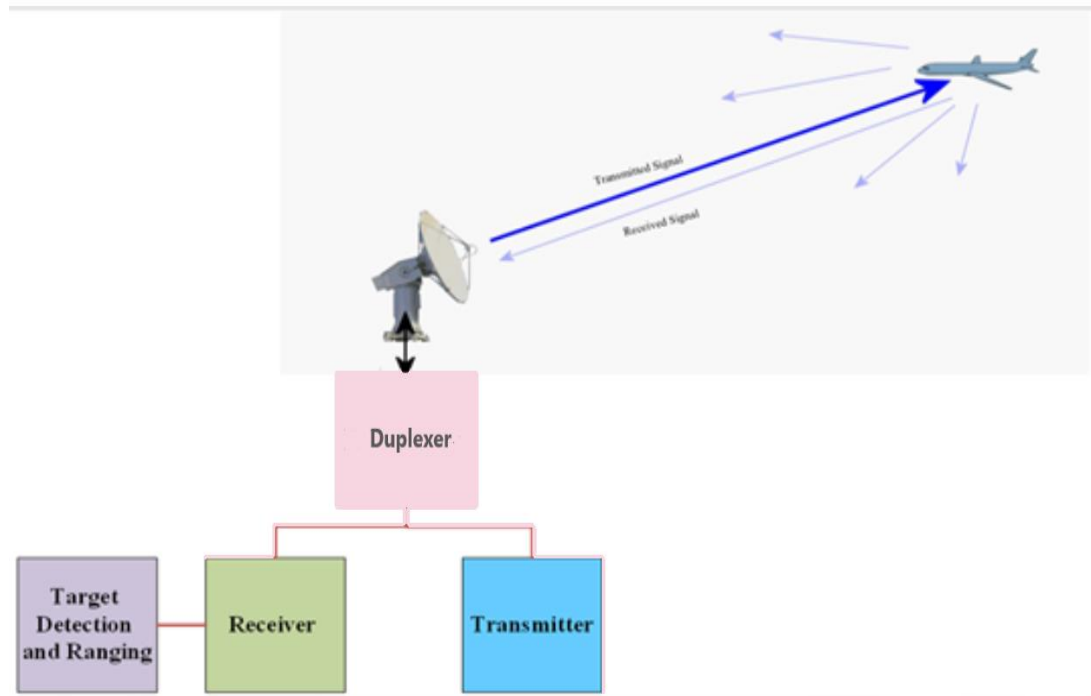


Figure 1.1: Radar Pulse Principle [2].

The radar can reveal the presence of these objects because the target may reflect electromagnetic radiation. On the other hand, the radar cannot detect the item if it does not remember radar signals [2]. This tendency is then used for the benefit of a particular defensive system. Microwave absorbent materials are widely used, and it is well understood that they can lower the power of electromagnetic waves as shown in Fig. 1.2 [3]. These microwave absorbent materials can be utilized outside or inside to reduce or eliminate reflections or transmissions from specified objects; this can also create an environment devoid of considerations or anechoic. Researchers have used several novel techniques to design a microwave absorber for many purposes [4]. This study briefly introduces metamaterial absorbers for microwave and optical applications. This research examined using fractal geometry as an absorber element for MMT in the

design of absorbers to increase the absorption rate and give a wide bandwidth suitable for numerous radio, microwave, and optical applications.

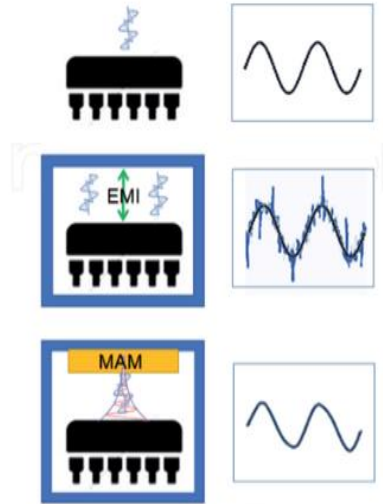


Figure 1.2: Microwave absorbers are used to minimize EMI [3].

Rapid technological advancements in radar detection systems have made radar absorption a critical problem today, necessitating the creation of methods for enhancing radar absorption. The primary defence challenge is concealing targets like aircraft, ships, missiles, and other defence vehicles. This challenge can be overcome by significantly reducing the target's radar cross-section. Whether the marks are vehicles or guided weapons, they can better avoid radar detection with reduced RCS. For example, shape, active cancellation, passive cancellation, and radar-absorbing materials have all been utilized to reduce the RCS. One of the most efficient methods to control RCS is shaping, including designing surface profiles or altering exterior features so that little to no radiation is scattered or reflected on the radar as shown in Fig. 1.3 [4]. However,

complete RCS control through shaping is not feasible due to several design restrictions. In most cases, a reduction is only possible in a small angular zone and comes at the price of higher RCS in other areas. Additionally, shaping is only effective at higher frequencies; in fact, it is practically useless at lower frequencies [5].



Figure 1.3: Microwave absorbers in military applications [4].

The B-2 Spirit stealth bomber, F-22 Raptor, F-35 Lightning II, and F-117A Nighthawk stealth fighter are excellent examples of shape. To decrease scattering from hotspot zones, passive and active cancellation use active/passive patches at the necessary spots on the target (where the reflections are maximum). But these techniques have something to do with the limited bandwidth and intricate system designs. The intricacy of designing active and passive filters and the aerodynamics issue have made RAMs crucial for obtaining radar absorption qualities. Because RAMs are widely employed for radar absorption, our work has also concentrated on them [5].

Radar Absorbing Material (RAM) technology is gaining popularity; radar-absorbing materials are coverings whose electric & magnetic characteristics have been chosen to facilitate the absorption of microwave radiation at discrete or wideband frequencies. In military applications, a vehicle with a small Radar Cross Section (RCS) may be necessary to avoid discovery while carrying out a covert operation [6]. Criteria have resulted in the developing of very low-observable or stealth technology, which minimizes the likelihood of an airplane being detected. The design of radar absorption materials is constrained by the legal capacity and mass of the surface covering. In addition, designing a broadband radar absorbent structure in a small volume is difficult. The analysis is carried out by computing the plane wave reflection coefficient at the exterior surface of the composite coating; using a computer program that selects layer parameters that determine low reflection coefficients for electromagnetic radiation under the constraints of limited layer thickness and maximum frequency bandwidth. The notion of absorbing incoming electromagnetic (EM) radiation by placing lossy material in the track of the waves is widely recognized [6].

There are several military applications, notably at microwave frequencies, such as reducing (RCS) on the outside of various military aircraft and vehicles by coating them with absorbent materials [7]. Expanding the volume of the material and changing its form can result in electromagnetic energy absorption over a broad bandwidth if unlimited space is considered. However, to guarantee that the ideal bandwidth and reflectivity properties are reached to match the requirements for military uses when space is constrained, as is typically the case for military applications, is a challenging design problem. There may be weight and volume restrictions on the absorber. Radar

absorbing materials, as the name directs, reduce the energy reflected by the radar through the absorption of incident electromagnetic radiation through ohmic loss in the medium, similar to how a resistor dissipates heat when an electrical current runs through it. The perfect absorber allows the incoming wave to pass through without reflection and swiftly reduces the tide in its internal to a minimal amplitude [8].

1.2 Literature Review

The fast advancement of communication technology in recent years has been recognized by scientists and engineers working on this subject. People have been inspired to use technological advances to improve their quality of life. Microwave absorbers are used in the electronics industry to diminish the presence of electromagnetic wave interference (EMI) and absorb it. This section of the thesis discusses and reviews past works related to our study, emphasizing the synthesized absorbing material and a sound absorber.

IN 2012, FAN Yue-Nong et al. [9] demonstrated a wideband, polarization-insensitive, wide-angle planar metamaterial absorber composed of a continuous resistive sheet, an electric resonator created from a MIK fractal loop structure, and a dielectric substrate. The suggested MA is more than 90% absorbed between 2.2GHz and 20GHz, according to simulation results. This absorber can be used in a variety of military contexts.

IN 2013, Yong-Zhi Cheng et al. [10] showed how they used resistive layers and fractal frequency selective surfaces to produce a wideband metamaterial absorber (MA). The absorption is wide-angle and polarization-insensitive, and the total thickness is only 0.8 mm. Thanks to the multiband resonance properties of the Minkowski (MSK) fractal loop structure and the Ohmic loss characteristics of resistive films, this composite MA exhibits numerically a considerably absorptive bandwidth of about 19 GHz in the range 6.51-25.42 GHz. This design offers a practical and efficient method to create a broadband absorber in stealth technology. This design provides a helpful way to widen the absorber's band.

IN 2015, Praneeth Munaga et al., [11] a broadband polarization-insensitive metamaterial absorber for C-band (4-8 GHz) applications presented using lumped resistors. The suggested structure's unit cell is built on an inverted Minkowski fractal loop, in which four lumped resistors are installed to provide a broad absorption band at the cost of a 5 mm thick dielectric substrate that is just 0.033o concerning the lowest operational frequency.

IN 2015, Somak Bhattacharyya et al. [12] presented an ultra-thin, compacted metamaterial absorber using a lone, square-shaped fractal structure as the unit cell. The fractal structure's geometrical parameters have been created in such a way that it displays absorption at 4.17 GHz and 11.16 GHz. The structure of the absorber has fourfold symmetry, which makes it polarization-independent. The construction is ultra-thin, with a thickness of just 1.6 mm.

IN 2016, Dingwang Yu et al. [13] in this study used the modified Minkowski (M-Minkowski) fractal structure to provide the foundation for the construction of the miniature metamaterial absorber. The top layer of the suggested absorber is an etched M-Minkowski fractal structure on a dielectric substrate, and the lower metal plate completes the design. The metamaterial absorber features dual-band absorbing peaks with a high absorptivity (>99 %). Compared to the Minkowski fractal structure, the suggested absorber can lower the absorption response bands and further apply to downsize.

IN 2018, Shicheng Fan and Yaoliang Song [14] presented a perfect metamaterial absorber based on fractals that is broadband polarization insensitive. The unit cell's bandwidth is increased by combining fractal and circular architectures. A simple equivalent circuit model explaining the absorption process was presented to anticipate the absorption frequency of the suggested absorber, according to the simulated result. In systems with rotational symmetry, the absorber is polarization-insensitive. Antenna design, electromagnetic interference, and radar target stealth are a few potential uses for this absorber, which is produced and tested in the X-band.

IN 2019, Francesca Venneri et al. [15] presented a fractal absorber for dual-frequency operating in the UHF band based on a metamaterial structure. The suggested fractal shape's shrinking abilities are employed to create a dual-band metamaterial absorber cell with a smaller size ($< \lambda/2$ at both operating frequencies) and a thin substrate thickness ($\approx \lambda/100$). In the vicinity of the ideal operating frequencies, firm absorption peaks (> 99 %) have been simulated (i.e., 878 MHz and 956 MHz). A fractal MA panel has been prototyped and experimentally confirmed, showing the capabilities

of the suggested design in accomplishing the ideal absorption condition under the dual-frequency modality, saving thickness and size over typical microwave absorbing configurations.

IN 2019, Ting Chen et al. [16] showed a fractal perfect metamaterial absorber with an ultra-wideband, polarization-insensitive tree-shaped microstructure with two dielectric substrates, a three-dimensional metal tree, and four lumped resistances. The polarized-insensitivity and wide-incident absorption properties of the suggested metamaterial absorber were fully light using near electric fields, angular absorptions, and surface current distributions. A perfect metamaterial absorber device was presented and measured in a microwave anechoic chamber utilizing a conventional printed circuit board approach. With an absorptivity greater than 80%. The broadband absorber can be used for stealth technologies and acoustic cloaks.

IN 2019, Mohamed Edries et al. [17] introduced a brand-new dual-band metamaterial absorber based on fractal geometry; it has two resonance frequencies of 2.24 GHz in the S-band and 7 GHz in the C-band, with absorption maxima of 97.2 per cent and 98 per cent, respectively. It has been shown that the electric field distributions and surface currents may explain how the suggested structure absorbs energy. The Computer Simulation Technology (CST) Microwave Studio produces all simulation results.

IN 2020, Alka Dileep et al. [18] presented a new metamaterial absorber for X-band applications based on Minkowski fractal patch design. In a single absorber, many unit cells with sizes tuned for resonance at tight space-out frequencies were employed.

The results of the entire wave simulation demonstrated the broadening of bandwidth achieved by utilizing dimensionally diverse fractals strategically placed on the absorber.

IN 2020, Qi Li et al. [19] proposed a P and L band functioning ultra-thin metamaterial absorber. A three-dimensional fractal tree topology loaded with lumped resistors is used to produce broadband absorption qualities. According to the simulation's findings, the suggested metamaterial absorber's working bandwidth is between 0.7 and 2 GHz. And its absorptivity is above 80%.

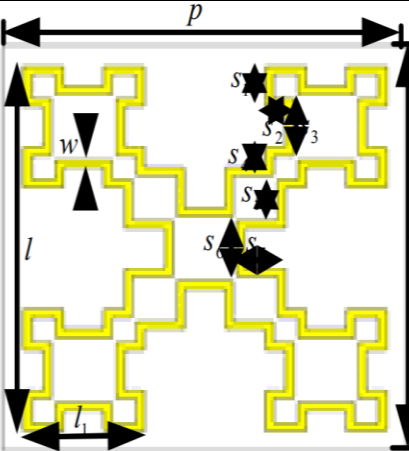
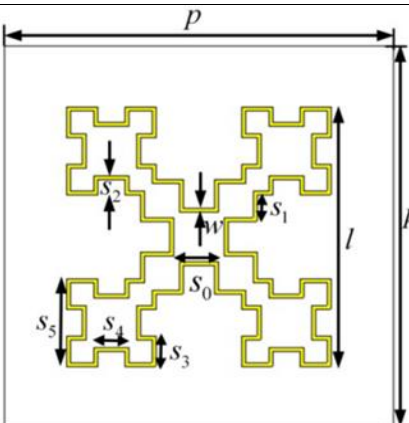
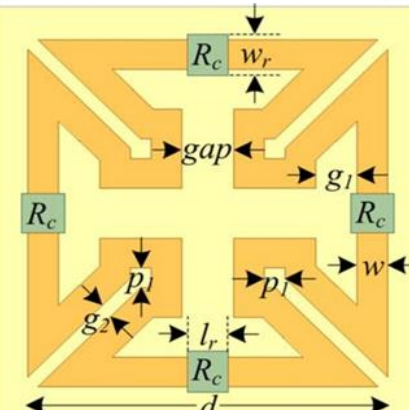
IN 2021, R. M. H. BILAL et al. [20] explored a mainly developed metallic (E-shaped fractal-based perfect metamaterial absorber) (PMA) with relatively broad absorptivity in the microwave regime's K- and (Ka-bands). The top surface of the PMA is made up of square-shaped split-ring resonators (SRRs) encircled by the fractal pattern. Transverse electric (TE) and transverse magnetic (TM) modes were used to evaluate the robustness of the suggested design. The SRRs have a capacitive effect at higher frequencies, whereas the fractal resonators do so at low frequencies. Findings from the simulation and the observations were reasonably comparable. The FMA achieves the highest absorptivity of ~80%. However, at particular operating frequencies, the structure shows near-perfect wave absorption.

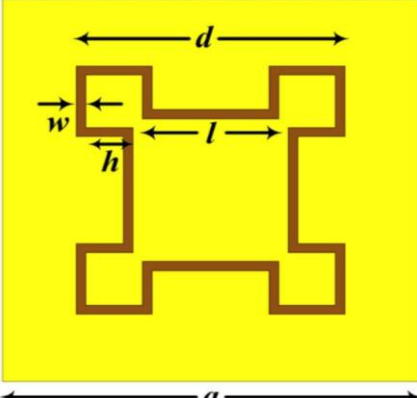
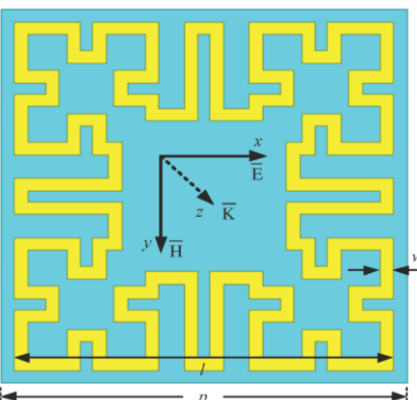
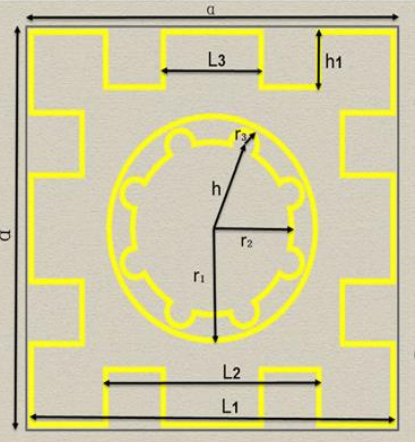
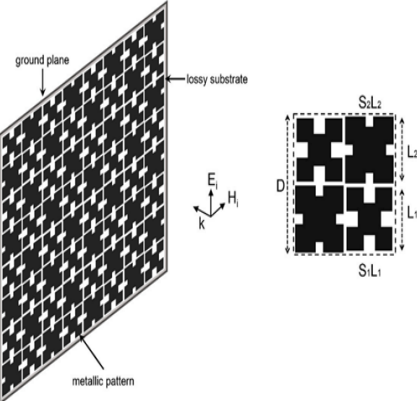
IN 2021, Akaa Agbaeze Eteng et al. [21] showed how to make a small unit cell absorber using second-order Minkowski-inspired fractal geometry; compared to similar microwave absorber cell geometries, the suggested unit cell has a footprint of 0.11λ . At the operational frequency of 2.45 GHz, the structure achieves a near-perfect absorption peak of 99%. As a result of this research, he discovered that structure might be used to

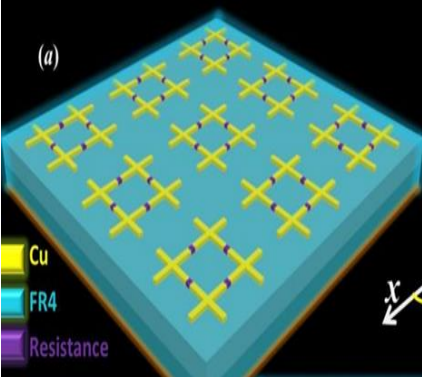
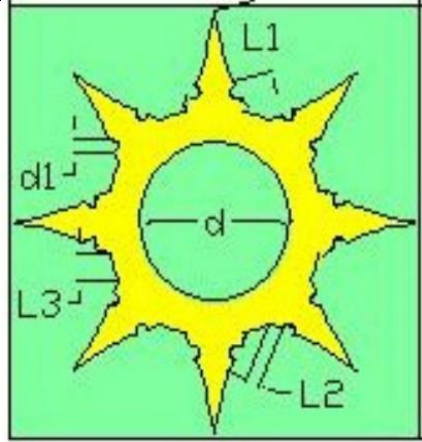
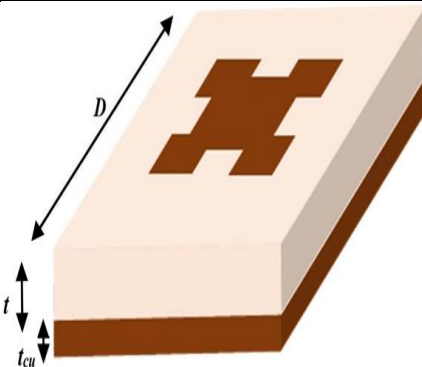
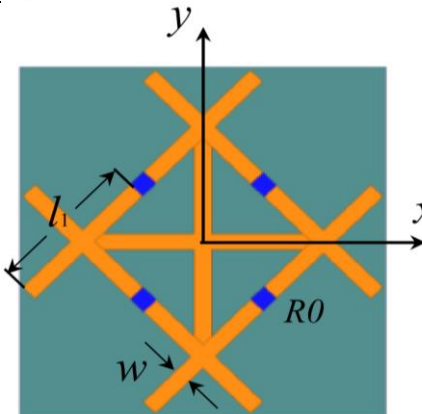
create absorber arrays to limit multipath effects and avoid eavesdropping assaults in indoor wireless situations.

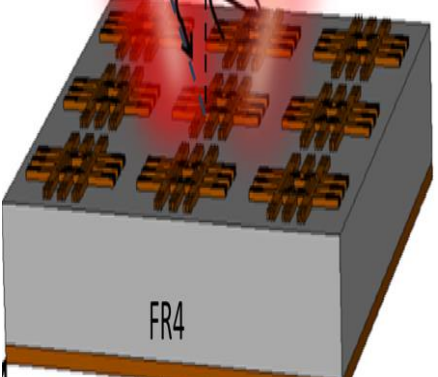
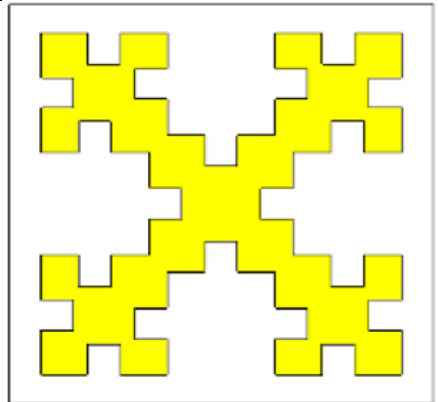
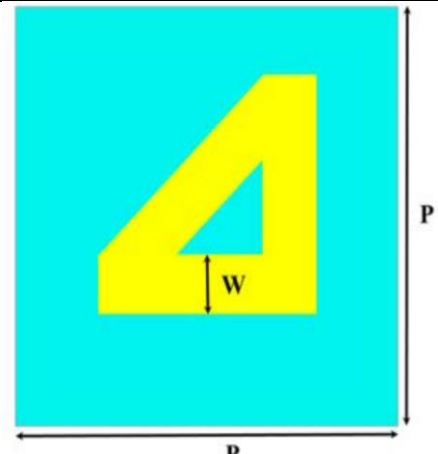
IN 2021, R. M. H. Bilal & M. A. Naveed et al. [22] designed a set square metamaterial absorber for X-band uses the X-band metamaterial absorber. In the current communication, the authors neglected to account for the cross-polarized reflection component in calculating the absorption. Additionally, it is demonstrated that the unit cell's isotropic shape is excellent for polarization conversion and has poor absorption.

Table 1.1: References fractal absorber designs associated with metamaterial from 2012-2021.

No.	Ref.	Shape of Metamaterial	Type of Fractal	Absorption	Frequency
1	[9]		Minkowski fractal (MSK)	90 %	2.2-20 GHz
2	[10]		Minkowski (MSK)	90 %	6.51-25.42 GHz
3	[11]		Minkowski fractal loop	97.7 %	4 - 8 GHz

4	[12]		square fractal (MSK) loop	99.1 & 99.7 %	4 - 16 GHz
5	[13]		Modified Minkowski (M-Minkowski)	99 %	3 - 15 GHz
6	[14]		fractal structures	99.45 %	8 - 12 GHz
7	[15]		Minkowski fractal	98.5 %	878 - 956 MHz

8	[16]		Three-dimensional fractal metal tree	80 %	3 – 15 GHz
9	[17]		Sun fractal	97.2 % & 98 %	1 - 7 GHz
10	[18]		Minkowski (MSK) fractal	80 %	8 - 12 GHz
11	[19]		fractal tree metamaterial absorber (FTMA)	80 %	0.5- 2 GHz

12	[20]		E-shaped fractal	96 %	20-30 GHz
13	[21]		Minkowski fractal	99 %	2 - 4 GHz
14	[22]		Metasurface fractal	80 %	7 - 13 GHz z

1.3 Statement of Research Problem

1. Traditional microwave absorbers are typically made of composite materials. These absorbers can show strong absorption over a relatively wide frequency

range if the thickness is sufficiently large. For a given absorption level, the frequency bandwidth usually decreases with a reduction in consistency. That brings a new way to improve the absorption property of the traditional magnetic absorber, especially in the low-frequency range under limited thickness.

2. Due to high negative magnetic permeability, magnetic materials can broaden the bandwidth of the absorber at a small thickness. One way to miniaturize the absorber is by using fractal geometry. Combining magnetic and metamaterials to design the absorbing body overcomes the disadvantage of large specific dimensions and increases the absorption bandwidth.

1.4 Scope and Motivation of the Project

One of the most critical points that have motivated researchers to work with metamaterial is that it is a new technology. Besides, the advantage that this technology has is significantly improving absorber performance.

1.5 Aim of The Work

- Designing a radar absorber with a small size and high absorption rate is one of the critical issues faced by previous researchers.
- The method of increasing the high-frequency bandwidth of absorption of microwave absorber almost without increasing the absorption rate and giving a wide bandwidth by

designing a kind of radar-absorbing material (RAM) based on metasurface with a thickness of less than 2 mm suit to X-band radar applications.

- Design of fractal geometry as an absorber element based on the principle of MMT technology to miniaturize the substrate thickness to be less than 2mm.

1.6 Research Contribution

This work contributes to the design of three proposed absorbers:

- 1- Design Apollonian Gasket Fractal based on Synthesized Absorbing Material Absorber of Unit Cell.
- 2- Design the proposed model that Modifies for Apollonian Gasket Fractal based on (the SAM) absorber of the Unit Cell.
- 3- Design of (SAM) Absorber Based on the Sun Slot Fractal Structure.

1.7 Thesis Outline

Chapter One: Introduction to Radar, Metasurfaces, Geometry of Fractals and Literature Review.

Chapter Two: Covers the Theoretical Background.

Chapter Three: Design of the proposed Synthesized Absorbing Material an absorber based on fractal geometry.

Chapter Four: This chapter discusses all simulated results for proposed absorbers.

Chapter Five: This chapter includes the conclusions of the proposed absorbers and future work recommendations.

CHAPTER TWO**THEORETICAL BACKGROUND****2.1 Theoretical analysis**

Radar is used for detection purposes; through the electromagnetic (EM) spectrum, visible, microwave, ultraviolet, infrared, and radio frequencies can be used in these systems. These electromagnetic waves determine the range speed, altitude, or direction of objects [23]. It is widely assumed that the Germans were the first to use (or study) radar absorber materials during World War II [24]. Civil and military applications generally need to prevent electromagnetic (EM) or microwave reflection [25-30]. To minimize the radar detection of an army vehicle using lossy dielectrics with definite scattering properties, which is the task of (RAMs) radar absorbing materials. The design problem may be viewed as achieving a lossy distributed network that matches the impedance of free space to that of the conducting body to the coating. (RAMs) are made up of compounds that absorb energy from electromagnetic waves that pass through them. Such materials have a complicated propagation constant with a fantastical element compensating for material loss. The dissipation of electromagnetic energy as heat is referred to as loss. There may be intrinsic molecular losses in many practical electric absorbers in adding to the loss owing to the material's limited conductivity.

A plane wave is an excellent approximation of most types of wave propagation [23]. In practice, electromagnetic waves from any source become plane waves as the space from the source increases. The most straightforward wave is the uniform plane wave, distinguished by the homogeneity of the fields in the plane parallel to the direction of propagation and by electric and magnetic fields that are mutually perpendicular to each other and the rule of propagation. The electromagnetic absorptivity of the surface structure is being tested in the current study using wave absorption incident normal to the target surface because it is a measure of power loss in the medium.

The loss tangent should be high for quick attenuation in the line length (or material thickness in this case) and must be set to provide the desired attenuation. The outside surface of the structure must be matched to open space in knowledge to achieve a reflection-free design. Alternatively, the outer surface reflection coefficient can be calculated as follows [24]:

$$\Gamma = \frac{Z_{in}-377}{Z_{in}+377} \quad 2.1$$

Γ : Reflection Coefficient.

377 ohms: Impedance of Free space.

The reflection coefficient with an ideal minimum value of zero can be chosen as a test function. Structures with the slightest reflection at fixed frequencies displayed a resonant reflection pattern.

Finally, the study showed that a comprehensive absorption bandwidth structure requires a typical distribution of layer parameters: a variation with a high dielectric constant at the metallic backplane moving to an approximately unit value at the layer between the air and the dielectric. Furthermore, the second layer farthest from the air/layer contact should have the lowest distribution of loss tangent. Adjusting the distribution of the layer characteristics in the structure, multilayered dielectric materials, or composite-based materials may minimize radio wave reflection across a broad range of frequencies.

2.2 Metasurfaces

Since they are used in a variety of applications, metasurfaces are a significant study issue. They can control electromagnetic radiation at microwave frequencies in a certain way. The advantages of the metasurface over other structures are its small weight, simplicity of manufacture, and ability to regulate waves using flat structures. Since the creation of frequency-selective surfaces and metamaterials, emphasis has been placed on the unique properties of distinct forms of metasurfaces. Surface impedance may be altered and managed by patterning the metasurface's unit cells, which has several uses in surface wave absorbers [31]. It is a kind of 2D metamaterial. A man-made structure known as metamaterial (MTM) can be created to produce the necessary electromagnetic response at a certain frequency. It's recognized as a group of man-made materials made of scattering components with negative permittivity and permeability. It may be characterized as a relatively homogenous material with a negative refractive index for the specified frequency range (i.e., the material's physical size is tiny in comparison to the electromagnetic wave's wavelength) [31].

The term “meta” is derived from the Greek word for “beyond.” Walser created the word “metamaterial” in 2001 to refer to “artificial materials” that perform beyond the boundaries of ordinary materials. Metasurfaces are surfaces that act as metamaterials, manufactured structures that can be tailored to produce the necessary electromagnetic response at specific frequencies. It is an artificial material made of scattering components with negative permeability and permittivity. It is a reasonably homogenous material (the material's physical dimension is tiny compared to the wavelength of the electromagnetic wave) with a negative refractive index for a specific frequency range [32]. V.G. Veselago [33] investigated the propagation of a plane wave through a material with negative permittivity and negative permeability in 1968. The negative permittivity or negative permeability indicates that electrons travel in the opposite direction when the electric field is applied. In the Veselago medium, the vector’s direction is opposite the phase velocity’s direction. This is in contrast to how standard material wave propagation works. This is why this type of media is referred to as Left-handed materials [34 - 36] and is seen in fig. 2.1 and fig. 2.2.

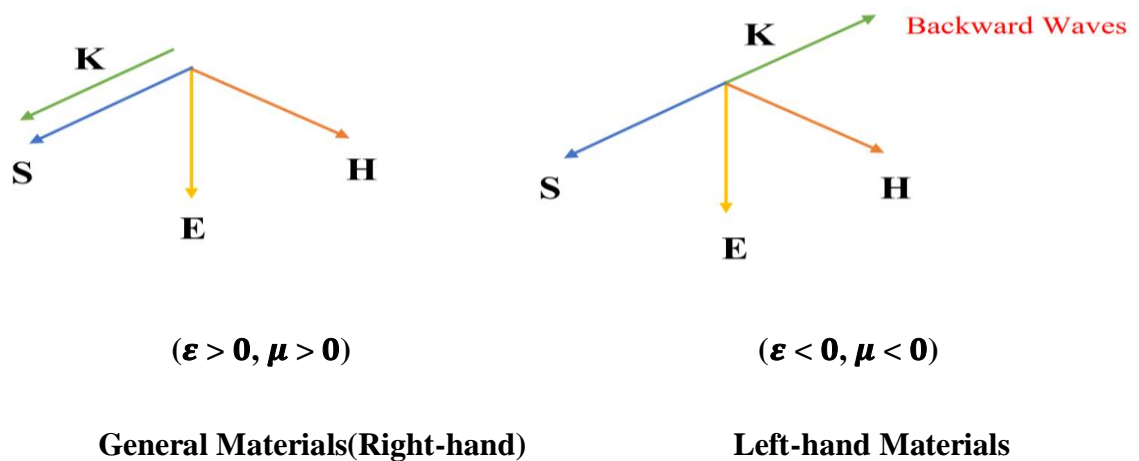


Figure 2.1: Electric – magnetic- surface wave and Poynting vectors of an electromagnetic wave in RH and LH mediums [24].

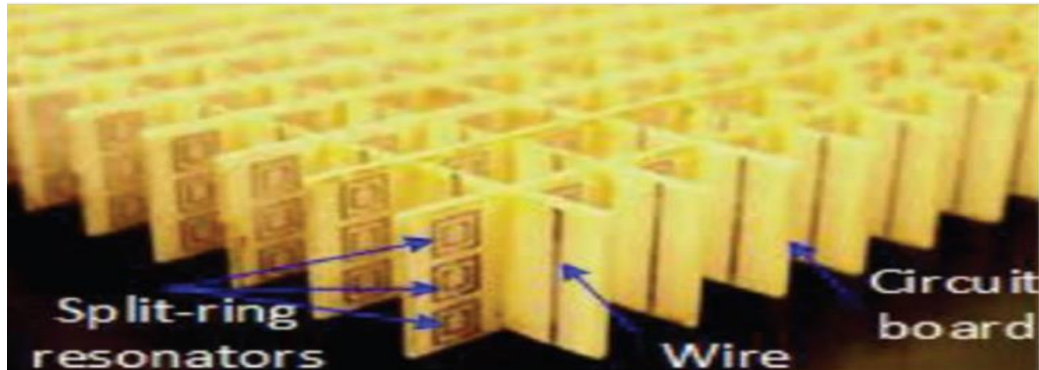


Figure 2.2: Collection of thin wires and SRR to shape DNG MTM [24].

It is first necessary to establish a material's permittivity (ϵ) and permeability (μ) as the characteristics employed in the interaction of electromagnetic waves to describe the electric and magnetic response. The permittivity defines how the dielectric medium affects and affects the electric field. This is an internal polarization test [37], often known as the medium's D (electric displacement) to E (electric field strength). The degree of magnetization of a material when a magnetic field is applied is known as its permeability [38]. The materials may be split into four categories, as shown in fig. 1.3.

Most materials have positive permittivity and permeability values and are referred to as “double-positive” (DPS) materials. The situation is referred to as “dual-negative (DNG)” if these values are negative. Epsilon-negative (ENG) materials exclusively have negative permittivity. Finally, negative permeability is a term used for

kinds with negative (MNG). Furthermore, no material in nature possesses both negative permittivity and permeability. As a result, they must be synthesized [39].

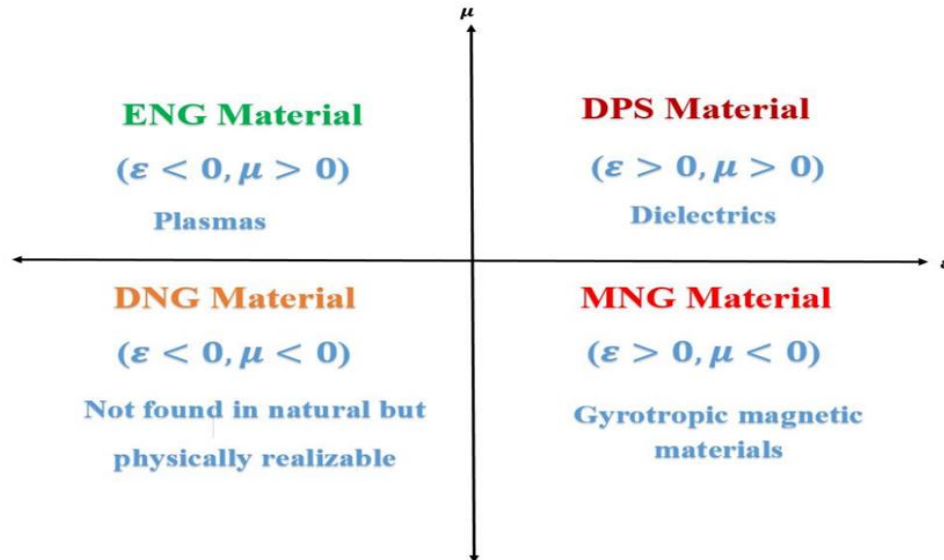


Figure 2.3: The four possible types of materials based on permittivity and permeability signs [39].

The hypothesis of a negative refractive index has validated a significant portion of the research. This branch of study has resulted in the development of the lens or super lens [40]. The super lens supports the capacity to concentrate on all propagation modes, and the image is obtained without loss of information. In mathematics, both ϵ and μ should have negative values to construct left-hand actions [41].

The refractive index is defined as the square root of the product of permittivity (ϵ_r) and permeability (μ_r), as shown below:

$$n = \pm \sqrt{(\epsilon_r \mu_r)} \quad 2.2$$

The value of n in the left-handed media is the refractive index and has a negative value. The (μ_r) represents magnetic permeability, whereas the (ϵ_r) Represents electric permittivity. There must be four alternative states of signs and $(+, +)$, $(-, +)$, and $(-, -)$, which lead to double-positive (DPS), single negative (SNG), or double-negative (DN) (DNG). Although permittivity and permeability are negative, the refractive index value will not seem negative till now. Still, it is feasible to demonstrate that choosing the square root leads to refractive index values near zero [42]. In a left-handed medium, the value of (n) is negative, and it can be driven by the phase (π) for both μ and ϵ . The importance of μ and ϵ in LH medium is given in terms of amount and step in the complex plane [43].

2.3 Geometry of Fractals

French mathematician B.B. Mandelbrot is credited with inventing the term “fractal” when he published “The Fractal Geometry of Nature” in 1970. He demonstrated that fractals function in non-integer dimensions and may properly depict irregularly shaped items or structures in nature that are not supported by Geometric forms, such as trees or mountains. By developing the idea of a fractional dimension, he created the word “fractal.” According to Mandelbrot, a fractal is a geometric entity broken into pieces, each of which is (roughly) a more miniature replica of the whole and may be repeated endlessly [44].

► Fractal Properties

Self-similarity and non-integer dimension are two of the most crucial features of fractals. The same is true with fractals: you may magnify them several times and see the same shape each time. It is more difficult to explain the non-integer dimension. Integer-dimensional objects such as 0-dimensional points, 1-dimensional lines and curves, 2-dimensional plane figures such as squares and circles, and 3-dimensional solids like cubes and spheres are all dealt with in classical geometry. On the other hand, many natural occurrences are best described by a dimension of two whole integers. The size of a fractal curve depends on how much area it takes as it twists and bends. The more a plane is occupied, the closer a flat fractal comes to two dimensions [45].

Mathematical fractal geometry has been known for over a century, and it is based on iterative equations, which are a type of feedback based on recursion. The Sierpinski carpet (a), Sierpinski gasket (b), Koch curve (c), and the MSK curve (d) are examples of these mathematical structures. The application of fractal principles in building an antenna and absorber minimizes the antenna or absorber size without sacrificing performance. Self-similarity, space-filling, and fractal dimension are three common aspects of fractal geometries [45]. It has been demonstrated that the self-similarity property of fractal forms may be used to create multiband fractal absorbers effectively and that the space-filling ability of fractals can be used to minimize absorber size. The fractal dimension feature has long been used to distinguish fractal geometries from Euclidean geometries. Fig. 2.4 shows some Mathematical fractal geometry examples.

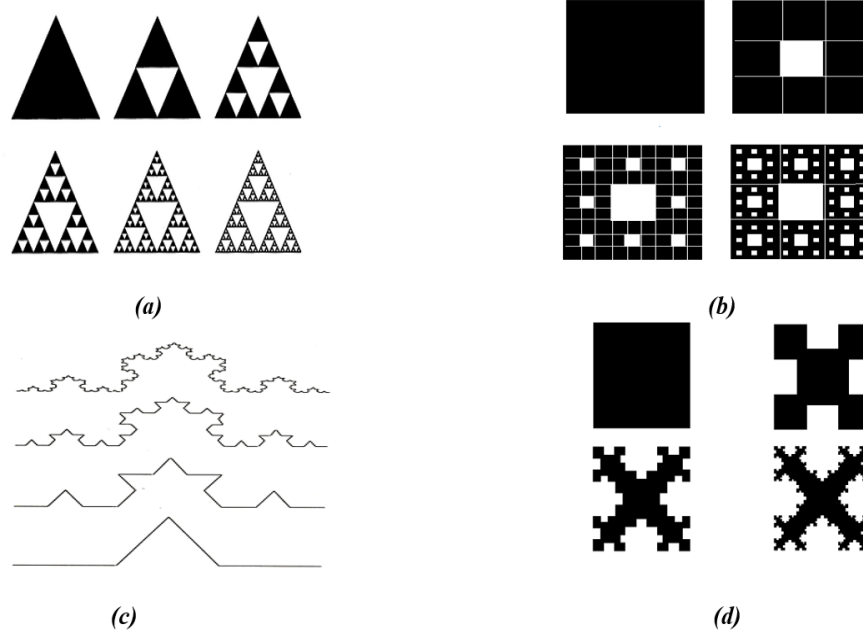


Figure 2.4: Mathematical fractal geometry examples, **(a)** Sierpinski Gasket, **(b)** Sierpinski Carpet, **(c)** Koch Curve, **(d)** Minkowski (MSK) curve [44].

2.4 Negative Refractive Index

The widespread concept of electromagnetic metamaterial (MTM) is an artificial and effectively homogeneous electromagnetic structure with unusual properties that do not occur in nature. One of the most critical conditions that must be provided to the effect that the design is homogeneous, the average unit cell size B must be smaller than guided wavelength λ_g [46]. Where B represents the cell size, the average cell size utilized in any structure must be $B < \lambda_g/4$, which means less than a quarter of a wavelength. To ensure refractive dominance over scattering-diffraction phenomena when an electromagnetic wave EM propagates into a metamaterial medium. The average cell size used in any structure will be indicated as an effective-homogeneity condition when it achieves $B < \lambda_g/4$ [46], where λ_g represents the guided wavelength.

As shown in Fig. 2.5, four potential signs are; (+, -),(+,+),(-,+) and (-,-) in the pair. While the first three signs are well known in traditional materials, the fourth sign (-,-) has a negative value for each of permeability and permittivity simultaneously. Compatible with new materials of the left-handed form (LH), Clearly left-handed structures are metamaterials. Depending on the description given above, called artificial material because the human hand made it, effectively homogeneous $B < \lambda g/4$, unusual properties appear ($\mathcal{E}, \mu < 0$) [46,47].

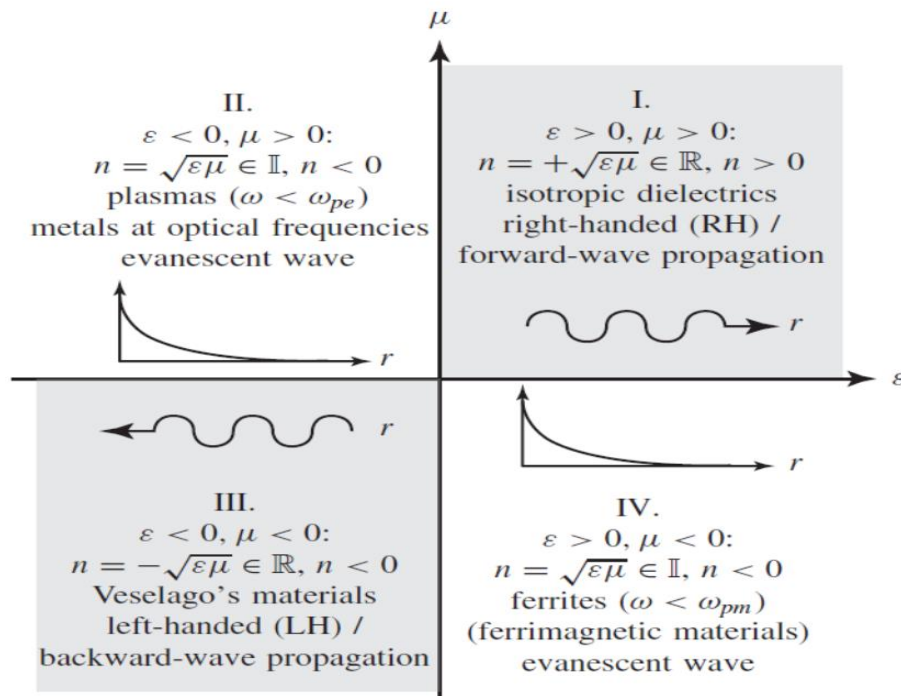


Figure 2.5: Material classification [46]. The angular frequencies: ω_{pe} and ω_{pm} : represent the electric and magnetic plasma frequencies, respectively. R, purely natural. I, strictly imaginary.

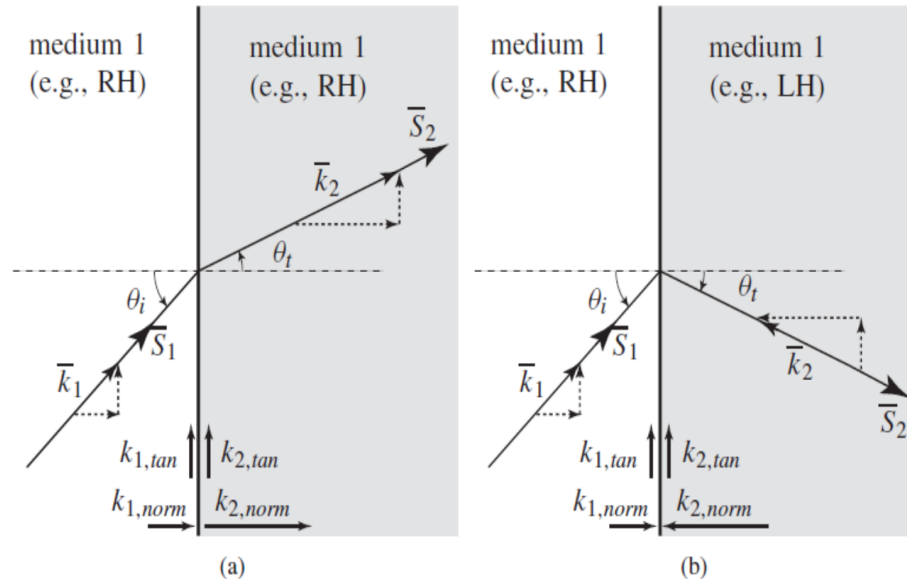


Figure 2.6: **(a)** Media with right-handed properties **(b)** Media with Left-handed properties [46].

The primary purpose of Fig. 2.6 is to illustrate the difference between the negative refractive index of Left-hand materials and the positive refractive index in right-hand materials only [46]. For materials with negative permittivity and permeability, one of the most important aspects is the concentration of waves. This characteristic plays a significant role in converting the metamaterial layer into a lens that focuses the electromagnetic waves travelling from the original absorber into plane waves and thus narrows the radiation beam's width, resulting in a good absorption increase.

2.5 Feeding Techniques

Many configurations can be used to feed metamaterial absorbers. The most popular is the Waveguide feed [48] to clarify the mechanism of the feeding method correctly and the main components that contribute to the basic design for this type of absorber. The following paragraph will include a detailed definition of this model with an illustration.

2.6 Waveguide feed

Waveguide port is the most common type of feeding method. Address in detail the use of this feeding method due to the consideration of the basic and significant role in extracting permittivity and permeability values from a single cell. Fig. 2.7 below shows the waveguide feed.

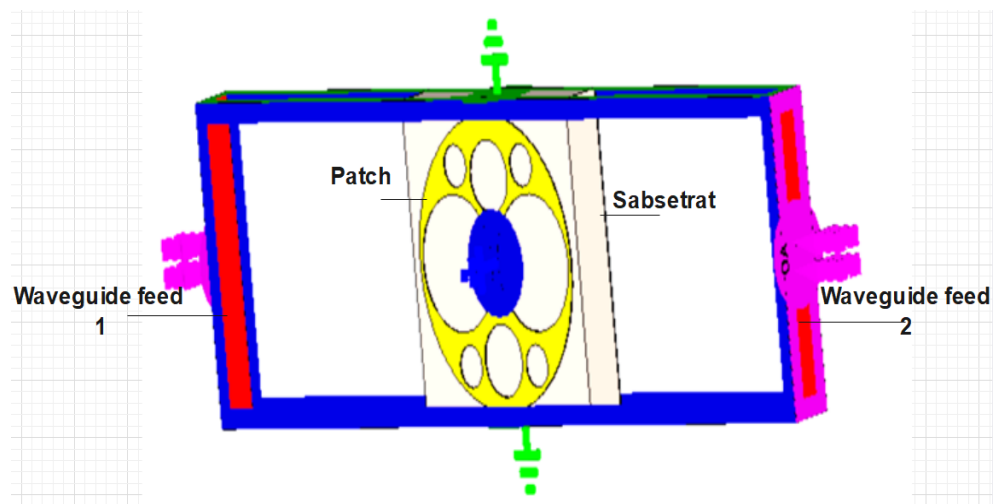


Figure 2.7: Waveguide feed.

2.7 Extraction of Metamaterial Parameters

In this section, the main metamaterial parameters that are used to describe the performance of the absorber are explained:

2.7.1 Method Definition

The design of metamaterial structures using commercial computer software is easily achieved and more convenient in this part by developing a step-by-step approach for obtaining the material properties. The curves for the complex permittivity and permeability of the metamaterial are calculated based on the unit element using a parameter-retrieval method utilizing the S-parameters. It uses CST to extract the S - parameters. The permittivity and permeability curves are calculated using a CST package. CST uses two methods to extract the S-parameters: perfect electric and magnetic (PE-PM) boundary conditions and master-slave boundary conditions [49,50]. Metamaterials are often created by repeating an essential building element in a predetermined way. The Unit Element (UE), which specifies the fundamental characteristics of the metamaterial, is the basic building block. In a simulator, the metamaterial is modelled and simulated by adding periodic boundary conditions applied to the borders of the unit element; it is assumed that the metamaterial is created by an infinite array of the unit element in the direction of the periodic boundary conditions [49,50,51]. The selection and design of a Metamaterial depend on the application and available resources.

The metamaterial can be correctly designed using full-wave analysis, but it is time-consuming. On the other hand, a priori knowledge of the electromagnetic properties of the material will accelerate the design procedure. The electromagnetic properties, such as the complex permeability (μ) and the permittivity (ϵ), can be evaluated either by the analytical Drude-Lorentz model [50,52] or by the S-parameter-retrieval method [50]. The Drude-Lorentz approach is inaccurate, especially when the metamaterial's unit element has a complicated structure. On the other hand, the S-parameter-retrieval process depends on the S-parameters recovered from the natural design and hence gives more precise values for the permittivity and permeability. I'll use this approach in this work. The S- parameters will be obtained from the trustworthy and widely used CST [50].

2.7.2 Mathematical Formulation

Permittivity, permeability, and conductivity are electromagnetics parameters that determine a material's properties; table 3.1 displays these definitions. The propagation profile of the material at each frequency is defined by the extraction of these values at various frequencies. In the extraction method used in this work, the refractive index and impedance of the material are used to extract the permittivity and permeability of the material under test [49,50]. To remove these material parameters (ϵ and μ), consider the unit element of a metamaterial with lattice vectors in all three dimensions. Appropriate boundary conditions and excitations are assigned to the

different surfaces of the three-dimensional unit element to simulate the periodic metamaterial and excitation of this metamaterial to extract the S-parameters [49,50,53].

The ratio ϵ''/ϵ' is known as the dielectric loss tangent, and it is commonly written as such; the loss tangent is additionally defined as:

$$\tan \delta = \epsilon''/\epsilon' \quad 2.3$$

A larger amount of absorbing material can be analyzed as a transmission line segment with an impedance (η) that looks as this:

$$\eta = \sqrt{\mu/\epsilon} \quad 2.4$$

Where: μ is permeability and ϵ is the dielectric permittivity as:

$$\mu = \mu' - j \mu'' \quad 2.5$$

$$\epsilon = \epsilon' - j \epsilon'' \quad 2.6$$

Where: μ' is natural permeability, μ'' is imaginary permeability.

ϵ' is real dielectric permittivity, ϵ'' is imaginary permittivity.

The permeability (μ) and permittivity (ϵ) are related to impedance and the refractive index by the following expressions illustrated in equations (2.4 - 2.8) [46]:

$$\epsilon = \frac{n}{Z} \quad 2.7$$

$$\mu = nZ \quad 2.8$$

Where: Z impedance of wave, n refractive index, μ_r and ϵ_r The relative permeability and permittivity which linked to a free space permeability and permittivity by [46]:

$$\mu_o = \frac{\mu}{\mu_r} = 4\pi * 10^{-7} \quad 2.9$$

$$\epsilon_o = \frac{\epsilon}{\epsilon_r} = 8.854 * 10^{-12} \quad 2.10$$

The absorptivity $A(\omega)$ can be calculated using the following formula [46]:

$$A(\omega) = 1 - |R(\omega)|^2 - |T(\omega)|^2 \quad 2.11$$

$$A(\omega) = 1 - |S_{11}(\omega)|^2 - |S_{21}(\omega)|^2$$

Where : $R(\omega)$: reflection coefficient

$T(\omega)$: transmission coefficient

When $(|S_{21}(\omega)|^2)$ equal to zero, the final equation is:

$$A(\omega) = 1 - R(\omega)$$

$$A(\omega) = 1 - |S_{11}(\omega)|^2 \quad 2.12$$

The standard radar received power equation can be stated as follows [54]:

$$P_R = \frac{P_T G^2 \sigma_t \lambda^2}{(4\pi)^3 d^4} \quad 2.13$$

where the P_T stands for the transmitting source, G is the antenna gain of the receiver, d is the distance between the radar and the transmitting source, σ represents the cross-section of the radar, and λ is the wavelength of the operating frequency.

This equation considers the target body made of conventional materials. In other words, the materials that cannot absorb the incident EM signals are reflective materials. However, if the body is coated with absorptive materials, eq. (2.13) should be modified to include the absorption coefficient as in eq. (2.14) to be as [47]:

$$P_R = \frac{P_T G^2 \sigma_t \lambda^2}{(4\pi)^3 d^4} (1 - A(w)) \quad 2.14$$

Eq. (2.14) is useful to predict and explain the absorption coefficients in the next chapters. As can be seen, when $R(w)=0$ (i.e., no reflection), the term $(1-A(w))$ becomes zero; then no power is received at the radar. In contrast, when $R(w)=1$ (i.e., full reflection), the term $(1-A(w))$ is the highest value. Then, the maximum power is received at the radar. Several factors affect the power reflection in our proposed design such as the substrate type, the synthesized geometry of the fractal curves, etc.

2.7.3 Simulation and Extraction of Results

To ensure that the engineered metamaterial layer includes negative permittivity and permeability properties, as well as the refractive index at the frequency at which the original absorber operates, thus guaranteeing a beneficial contribution to the original absorber's characteristics of the metamaterial layer and achieving the best performance

in the absorber. This procedure is carried out by installing the unit cells first, which is the main component of the design on a substrate sheet slightly larger than the size of the unit cell patch surrounded by sufficient boundary conditions; such as perfect electricity on the X-axis, perfect magnet on the Y-axis, and two Z-axis waveguide ports in some designs and another design put excellent electricity on the Y-axis, perfect magnet on the Z-axis, and two X-axis waveguide ports to extract results. Finally, achieve the extraction for permittivity, permeability, and refractive index. The S-parameter algorithm uses reflection and transmitted confection to get wanted curves [50,55]. Fig. 2.8 below shows the full details of a single unit cell to reach the required curves.

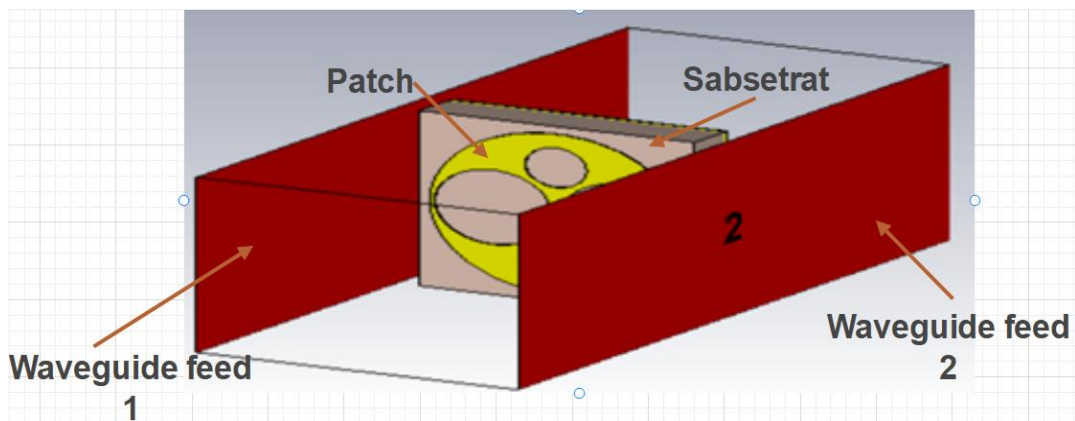


Figure 2.8: Unit cell between two waveguide ports.

2.8 Apollonian gasket fractal geometry

We summarize the mathematical process used to create the conventional Apollonian gasket illustrated in [56]. A specific type of fractal named an Apollonian

Gasket is made up of a collection of circles that are all closely tangent to one another and overlap inside a single large circle. As shown in Fig. 2.9 [57], there are several different types of an Apollonian Gasket, including (a) the Apollonian window, which is the single status with symmetry D_2 , (b) the general gasket, which lacks mirror symmetry, (c) Apollonian strip, which is a private status of the non-compact, and (d) regular threefold gasket, which has symmetry D_3 . Consider three identical circles arranged in a triangle or big circle so that each process is tangent to the other two, making a closed region and a curved triangle, to create the Apollonian fractal Fig. 2.9 two circles are perpendicular to these first three.

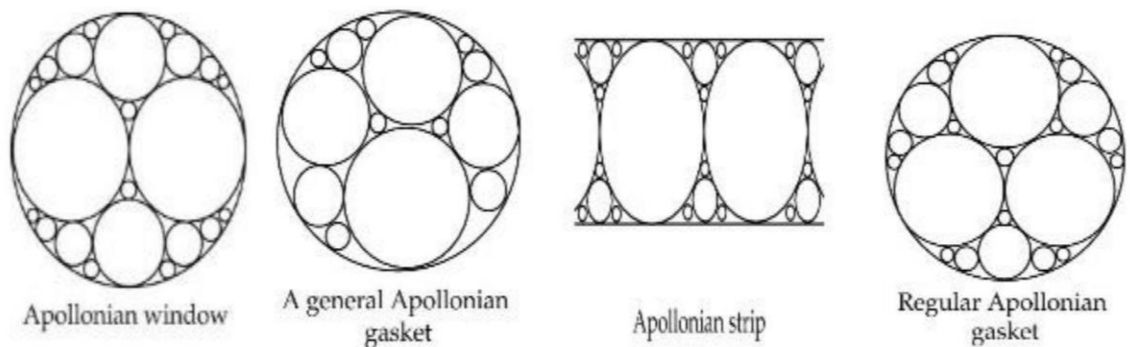


Figure 2.9: Different shapes for an Apollonian Gasket [57].

The following steps result in an Apollonian Gasket [57,58]:

- 1- Begin by drawing a large circle with a radius of r .
- 2- Everyone inside it touches the circle. There is a sideways tangent.
- 3- In the spaces between these circles, create smaller, as large as possible circles, taking care not to overlap any of the nearby ones.

4- Continue in this manner, inserting a circle as big as it can be without overlapping into each brand-new space.

In this thesis, we formed the second iteration Apollonian window fractal, as shown in Fig. 2.10. The largest circle has a radius of 2.5 mm. At the same time, the second next large circles have a 1.25 mm radius value. Finally, the two last small circles have a 0.83 mm radius value.

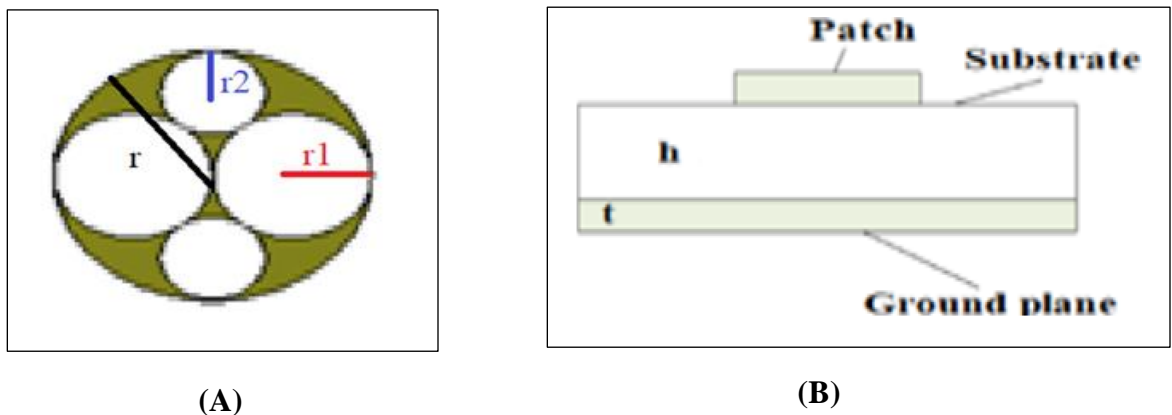


Figure 2.10: Structure of the proposed material fractal absorber

(A) Front view, (B) Side view.

CHAPTER THREE

DESIGN CONFIGURATION

3.1 Introduction

This chapter deals with the designs of metasurface absorbers based on fractal geometry. After that, underline the importance of high absorption and the most effective technique used to boost absorber performance. Then, in addition to clarifying the process to ensure the design is metasurface, describe a method used to feed the absorber. And the last step discussed in the chapter is the designs based on metasurface absorbers with complete details about the dimensions of different fractal geometries.

3.2 Research Methodology

In this section, the methodology will be introduced as shown in the flowchart, depicted in Fig. 3.1. The flowchart starts with selecting the appropriate application of the proposed absorber. Then, it continues to describe all steps followed in the thesis process such as selecting the substrate material and the Fractal curve type and iteration. The boundary conditions which are the perfect electric and perfect magnetic are set to mimic an infinite array of unit cells. After making the setup for the design to be ready for simulation, the design will be analytically simulated to obtain the S_{11} , S_{21} , S_{12} , and S_{22} . If the design has no good results, its dimensions will be tuned and optimized to re-simulate it again. Finally, plotting the absorption coefficient is made to demonstrate

how the design can confine the power inside it. Also, the current distribution is plotted to show where the power will be confined on the structure.

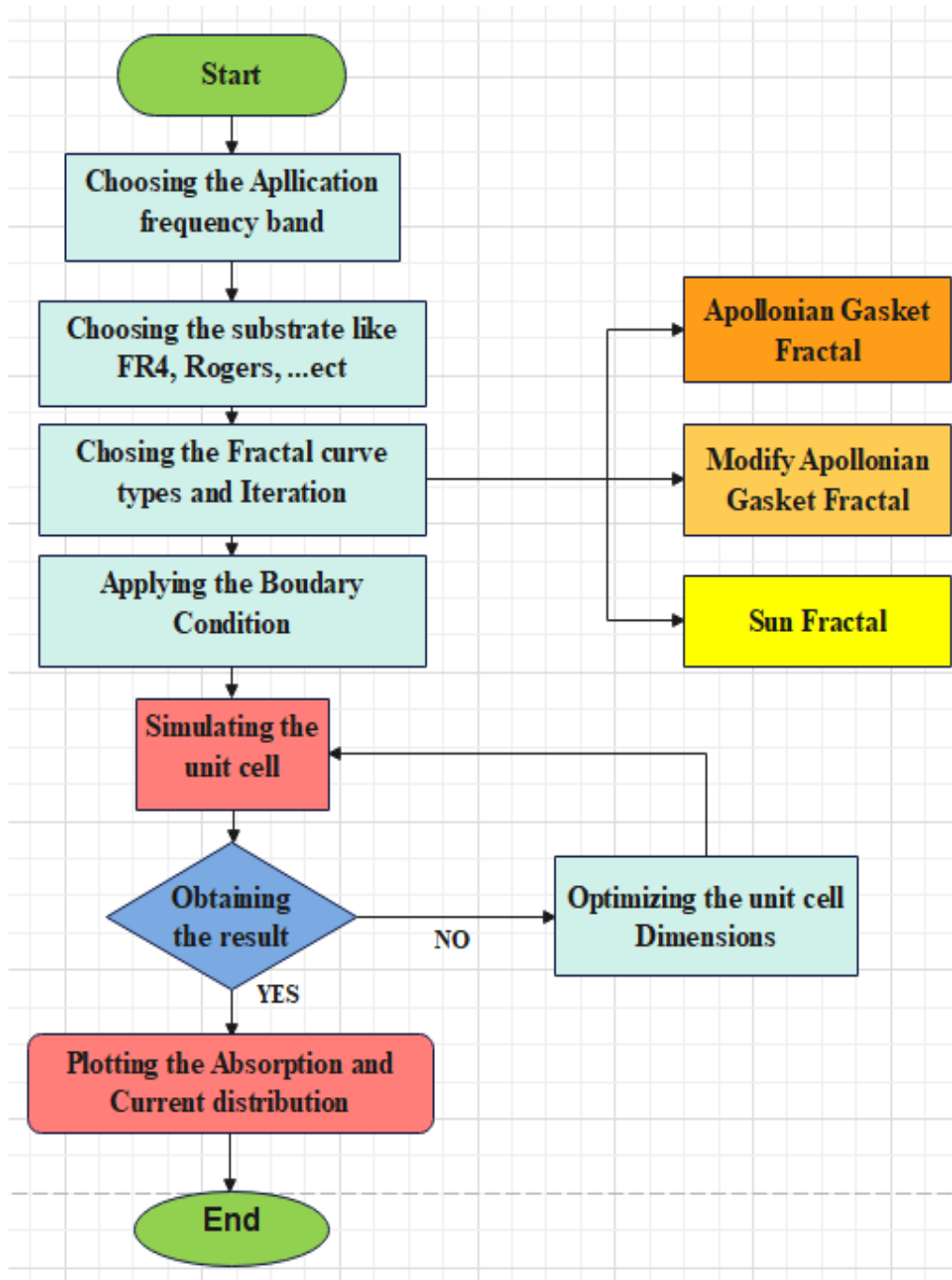


Figure 3.1: Shows the Flowchart of the Methodology of the Proposed Absorber.

3.3 The Proposed Model (I): Apollonian Gasket Fractal-based Metasurface Absorber of Unit Cell.

The design of a proposed metamaterial fractal-based absorber is displayed in Fig. 3.2. The proposed absorber is fed, which is the main component of the strategy on a substrate sheet slightly larger than the size of the unit cell patch surrounded by sufficient boundary conditions, such as put unit cells on the X-axis, unit cells on the Y-axis, and put openly on z-axis waveguide ports. Fouquet boundaries (number of fluquet modes = 2) to finally achieve the extraction for permittivity, permeability, and absorption. The substrate is FR4 with a thickness of $h= 1\text{mm}$, loss tangent 0.025, and dielectric constant $\epsilon = 4.3$. The dimensions of absorber parameters are mentioned in Table 3.1; all sizes are in mm.

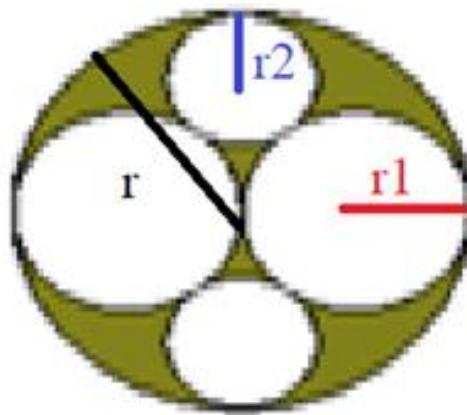


Figure 3.2: Proposed absorber structure.

TABLE 3.1: Design parameters of the proposed Apollonian gasket fractal Metasurface Absorber unit cell.

No.	Symbol	Quantity	Dimensions(mm)
1	r	The radius of the largest circle	2.5
2	r_1	The radius of the next two large circles	$r/2$
3	r_2	The radius of the last two small circles	$0.33*r$
4	t	The thickness of metallic elements	0.035
5	h	The thickness of the substrate	1

3.4 The Proposed Model (II): Modify for Apollonian Gasket Fractal-based Metasurface Absorber of Unit Cell.

The metasurface-based absorber has a structure resembling patchwork cells. As we'll see in more detail later, it is displayed in Fig. 3.3. The purpose of utilizing such a periodic metamaterial structure is to improve various absorber performance metrics, such as bandwidth and absorption. The suggested absorber has many different degrees of freedom to enhance its capabilities since the metamaterial layers are built up of 3D distributed copper metallic unit cells, which is the main component of the design, on a substrate sheet slightly larger than the size of the unit cell patch surrounded by sufficient boundary conditions, such as putting electricity on the X-axis, magnetic on the Y-axis, and putting open on the z-axis waveguide ports, to finally achieve the extraction for permittivity, permeability, and absorption. The substrate is FR4 with a thickness of $h = 0.5\text{mm}$, a loss tangent of 0.025, and a dielectric constant $\epsilon = 4.3$. The dimensions of the absorber parameters are mentioned in Table 3.2. All sizes are in mm.

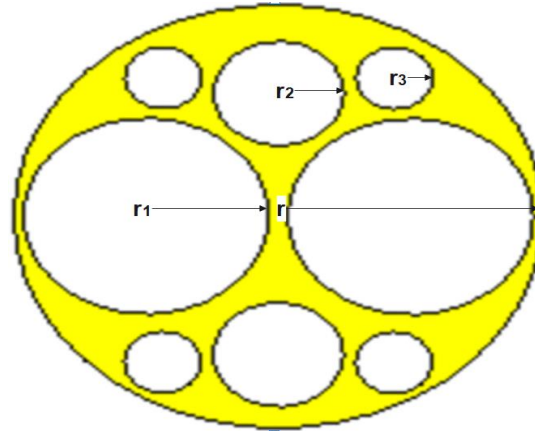


Figure 3.3: Proposed absorber structure.

► Unit cell & iterations:

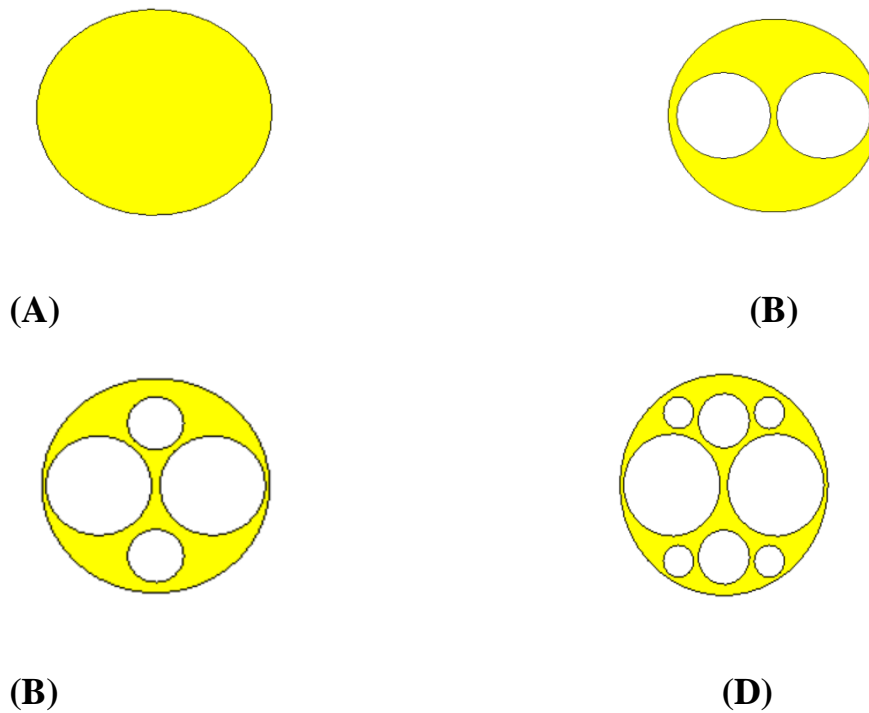
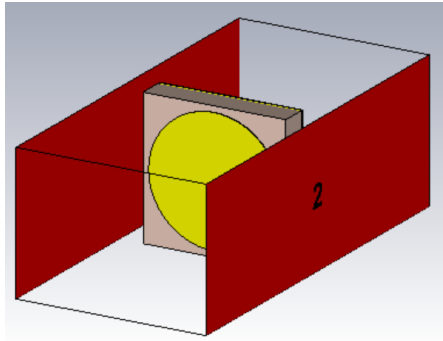
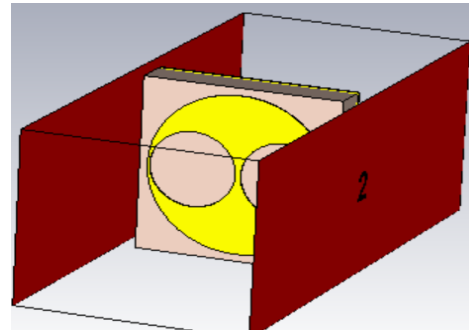


Figure 3.4: Different iteration stages of Apollonian Gasket fractal structure of the proposed fractal absorber (A) 0th iteration, (B) First iteration, (C) Second iteration, and (D) Third iteration.

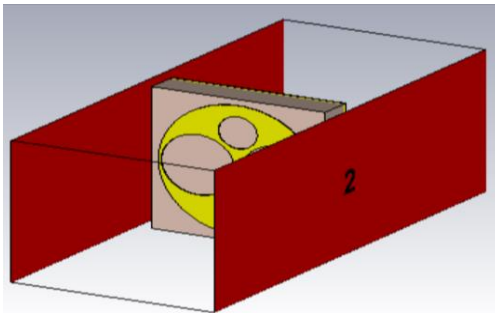
► Waveguide feed of iterations:



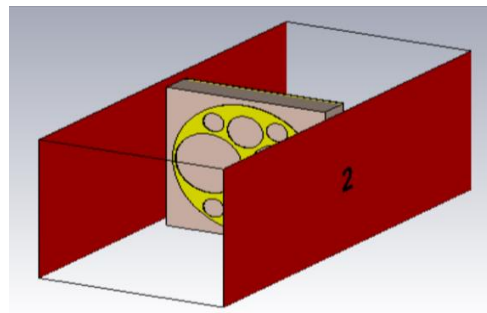
(A)



(B)



(C)



(D)

Figure 3.5: Waveguide feed of Apollonian Gasket fractal structure of the proposed fractal absorber (A) 0th iteration, (B) First iteration, (C) Second iteration, and (D) Third iteration.

TABLE 3.2: Design parameters of the proposed Apollonian Gasket fractal Metasurface Absorber unit cell.

No.	Symbol	Quantity	Dimensions (mm)
1	r	The radius of the largest circle	2.5
2	r_1	The radius of the next two large circles	$0.66*r$
3	r_2	The radius of the last two small circles	$r/2$
4	r_3	The radius of the last four small circles	$0.33*r$
5	t	The thickness of metallic elements	0.035
6	h	The thickness of the substrate	0.5

3.5 The Proposed Model (III): Design of Metasurface Absorber Based on the Sun Fractal Structure.

The structure of the proposed metasurface absorber is depicted in Unit Cell Structure Design in Fig. 3.6. The metamaterial absorber's structural design consists of a big outer ring, a sun-fractal copper form, and a continuous copper ground plate, each with a thickness of 0.035 mm and a conductivity of $\sigma = 5.96 \times 10^7$ S/m. A lossy dielectric substrate flame retardant (FR-4), which has a dielectric constant of 4.3, a loss tangent of 0.025, and a thickness of $h = 1$ mm, was used to isolate the fractal form from the ground plate. The suggested metamaterial absorber measures $50 \times 50 \times 1$ mm³ in total. Table 3.3 provides an example of the proposed unit cell's design parameters.

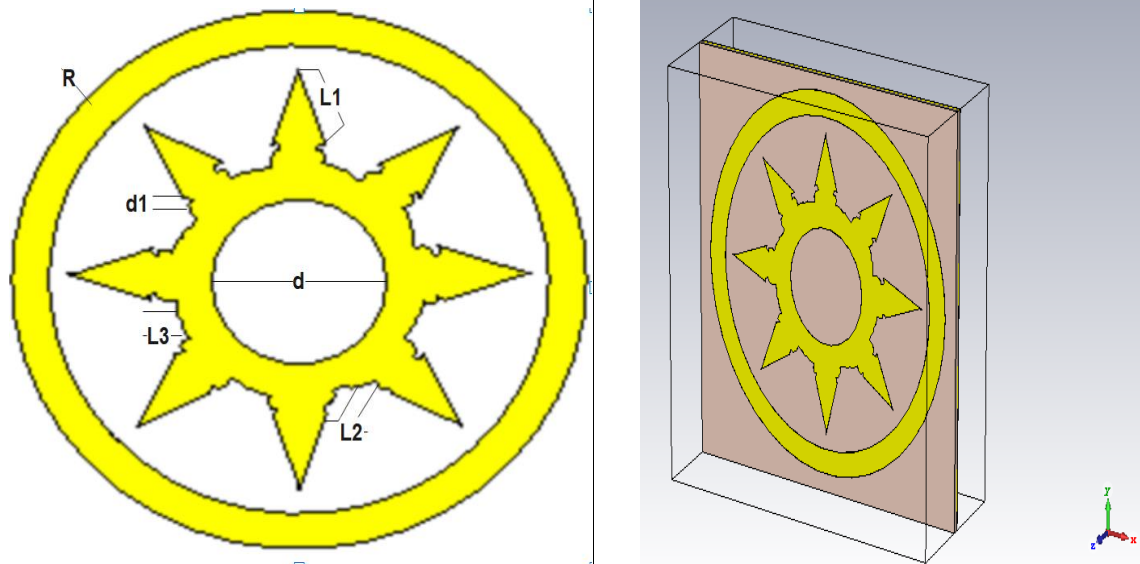


Figure 3.6: Sun fractal absorber metasurface structure proposed.

TABLE 3.3: The proposed Sun Fractal Metamaterial Absorber unit cell design parameters.

No.	Symbol	Dimensions (mm)
1	R	20
2	d	14
3	d1	3.5
4	L1	15
5	L2	3
6	L3	8
7	h	1

CHAPTER FOUR**RESULTS AND DISCUSSIONS****4.1 Introduction**

In this chapter, the results of the proposed absorbers introduced in the previous chapter will be demonstrated to show how our proposed designs can absorb and confine the incident EM signals inside them instead of reflecting or transmitting them. The designs are examined to show which parts are the main ones responsible for absorbing the EM signals. When changing the absorber's dimensions, the absorption performance will be affected, so the dimensions play a vital role in determining our design absorption. Therefore, the designs will be optimized to choose the best results. Moreover, not only the absorption coefficient will be presented, but also the scattering parameter S_{11} , permittivity, permeability, and the current distributions will be introduced to provide the overall performance evaluation. The computer simulation tool CST is utilized to numerically analyze the proposed structures depending on the integral equation algorithm. The periodic boundary conditions are applied to the side edges of the unit cells to mimic the array of unit cells making the infinite plane of the absorber. We examine the scattering parameters by designing the unit cells first, which is the main component of the design on a substrate sheet which is slightly larger than the size of the unit cell patch surrounded by sufficient periodic boundary conditions (the x and y

axes). The z-axis will be set as an open waveguide with a floquet wave port. In each simulation, the number of modes for each port is set as 2 (i.e., the TE and TM modes). The absorption coefficient is calculated using the S-parameters depending on equation (2.11-2.12) [55]. Finally, the absorbers are opaque for the transmitted waves (i.e., $S_{21} = 0$).

4.2 Study of the Apollonian Gasket Unit Cell Metasurface Absorber (I)

As demonstrated in the previous chapter, the proposed absorbers were carefully and accurately determined and designed. Then, the substrate thickness is altered, while the results are obtained as shown in Fig.4.1. The parametric study presented here provides a useful explanation of how the absorber performance can be influenced. However, all other design dimensions are fixed to only demonstrate the effect of the thickness of the substrate. As can be seen in the figure, the matching becomes very obvious when h is varied from 1mm to 5mm with a step of 1mm. The reflection coefficient S_{11} decreases rapidly when approaching the resonance frequency. This means that the impedances of the free-space and the absorber surface are almost equal to obtain good matching. The absorption becomes close to unity if both impedances are identical. Moreover, when $h=1\text{mm}$, the highest absorption is obtained, since the substrate dimensions highly control the absorber impedance. Also, other signal factors such as the polarization and the angle incidence governing the absorption but are out of the thesis scope.

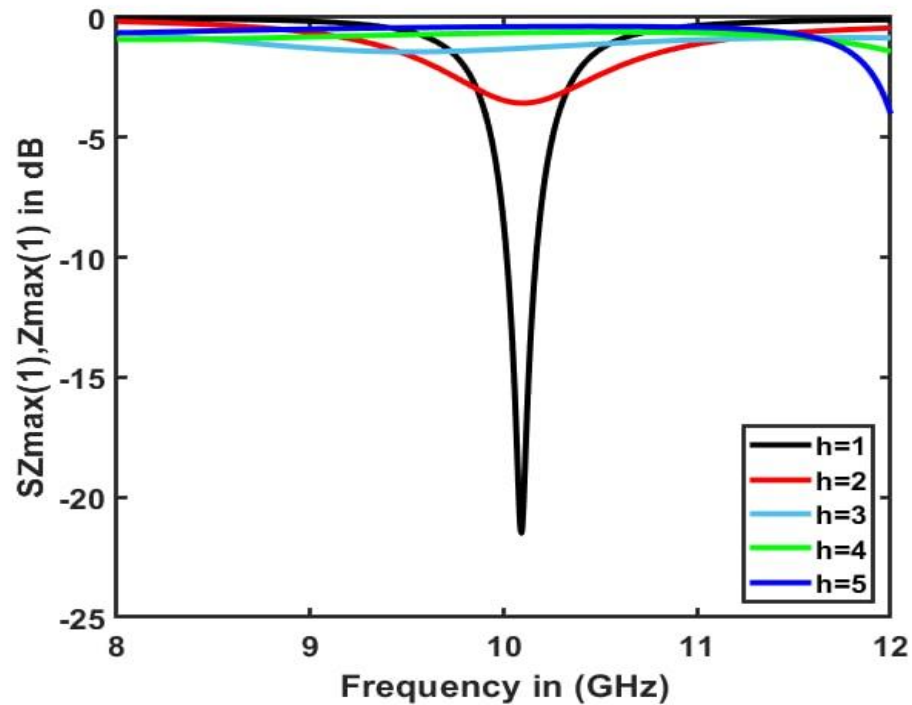


Figure 4.1: Parametric study of the Apollonian Gasket Fractal Unit Cell.

4.2.1 Extracting S-Parameter of the Apollonian Gasket Fractal Unit Cell Metasurface Absorber

The findings of the first design will be discussed in this section of the chapter, with the discussion focusing on the process for extracting the data that can guarantee that the design that was simulated in the CST is a design that depends on the metamaterial during construction. The results from the CST program appear for the cell from the suggested design, positioning it properly on the substrate, feeding it with a pair of waveguide ports, applying the boundary conditions from the unit cell on the X axis and Y axis, open on the Z-axis waveguide ports, and floquet boundaries (number of fluquet modes = 2), and extracting the values for the S-parameters. Fig. 4.2 below

displays all the method's outcomes. The simulation results of the proposed metamaterial absorber unit cell show the reflection coefficient S_{11} , which clearly presents a resonant absorption peak at 10.14 GHz which makes this absorber suitable for X-band radar applications with a bandwidth of 0.15 GHz. Typically, the bandwidth is determined when the $S_{11} = -10\text{dB}$. However, this does not mean that the absorber does not operate with a lower S_{11} . It still operates but with lower efficiency. The value of 6dB is the best limit for S_{11} . Fig. 4.2 demonstrates that the reflection decreases rapidly around 10.1GHz to obtain $S_{11} = -21.8\text{dB}$.

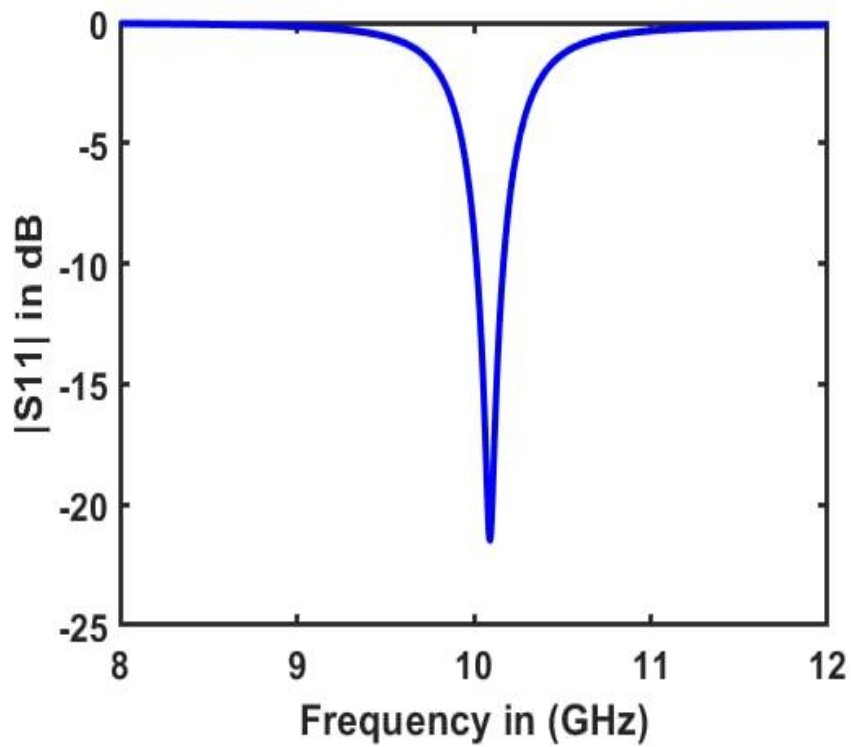
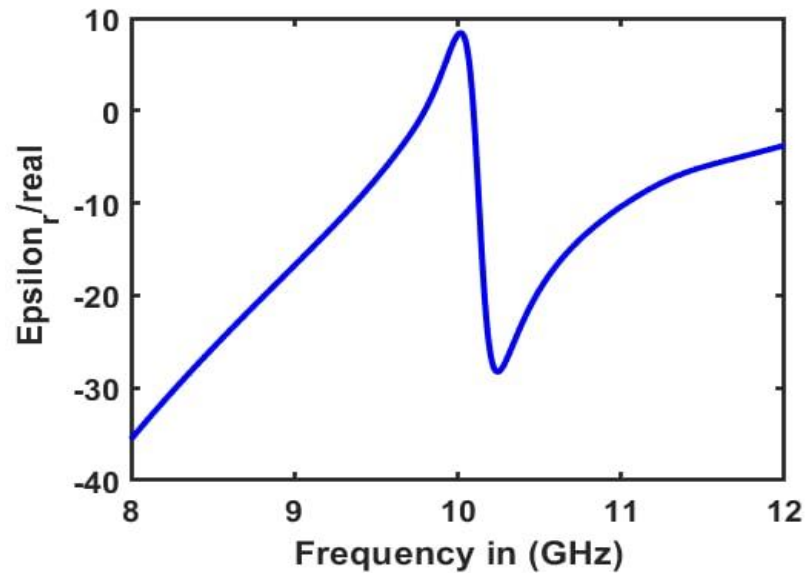


Figure 4.2: The S-parameters (S_{11}).

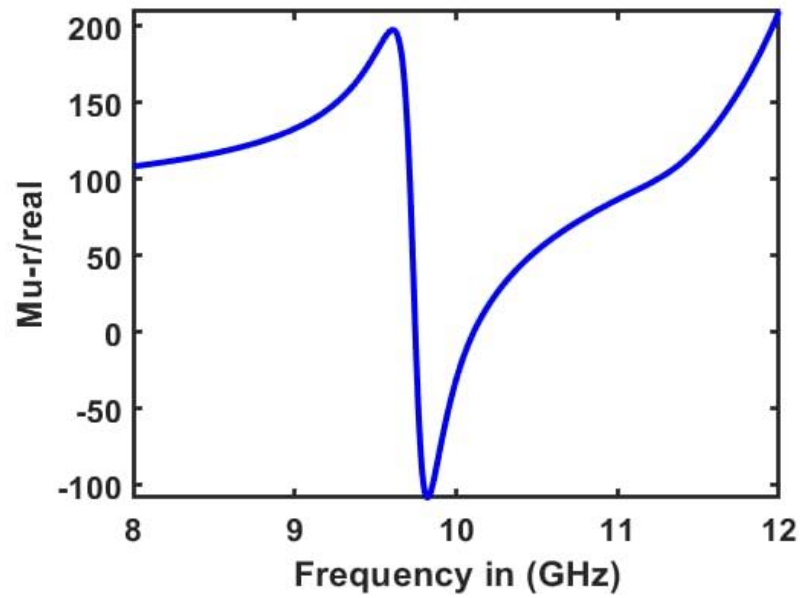
4.2.2 Extracting Permeability and Permittivity from the S-Parameters.

The CST software has the ability to extract the constitution parameters (i.e., the permittivity ϵ and permeability μ) from the scattering parameters S . The algorithm used to calculate these two parameters is given in detail in [59]. These two parameters will be used to calculate the refraction index n . As known, the scattering parameters function with the frequency, so the constitution and the refraction index are functions with the frequency as well. The refraction index changes from negative to positive values crossing the zero value. At the zeroth value of the n , the absorber structure will not reflect, refract, or either transmit the incident signals. Instead, the signals will be confined inside the absorber. Also, the constitution parameters are utilized to calculate the absorber impedance. When the impedance is equal to the free-space impedance, the matching occurs. In other words, the matching means that the signals enter the absorber without reflection.

No material in nature has negative permittivity and permeability at the same time. However, this is possible with the synthesized materials (i.e, metamaterials or 2D thin metasurfaces). The obtained material is called Left-Handed Material (LHM). In this material, the phase velocity and group velocity are in opposite directions. The material can also change its constitution parameters to obtain any value depending on the unit cell dimensions. The resulting parameters play a vital role in the absorption performance. Fig. 4.3 shows the ϵ and μ , and the results show that the absorber, at the resonance (X-band), inverts the ϵ and μ from the negative to positive or vice versa. The regions of the real parts of the ϵ and μ are negative where the peak absorption coefficient of the proposed absorber occurs.



(A)



(B)

Figure 4.3: (A) the permittivity (B) the permeability of metamaterial.

4.2.3 Extracting Absorption value from S-Parameters.

Fig. 4.4 shows the absorption coefficient which is about 0.997 or 99.7% at a frequency of 10.14GHz. When comparing the result with the S11, we can see that the absorption reaches its maximum value at the resonance, resulting in higher absorption. The value decreases as the frequency decreases or increases until reaching the lowest value closing to zero because at other frequencies the absorber cannot resonate.

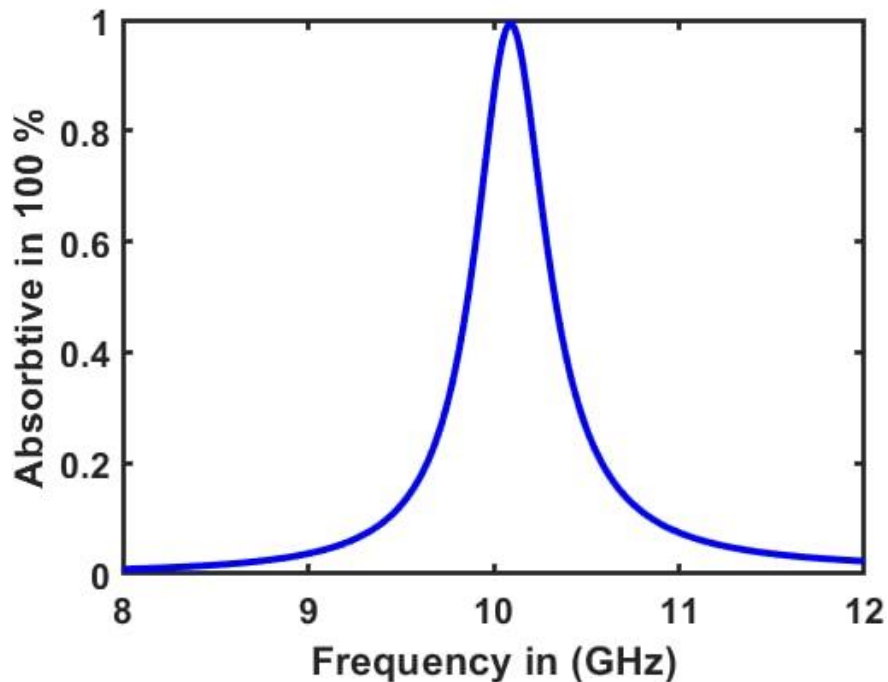


Figure 4.4: The Absorption value

4.2.4 Extracting the Refractive Index value from S-Parameters.

At the resonance, the n becomes zero, see Fig.4.5. Thus, the absorber confines the incident signals. At lower frequencies, the n is negative where this property enables

the design to violate Snell's law, whereas, at the higher frequencies, the n is positive which is the same as the natural material.

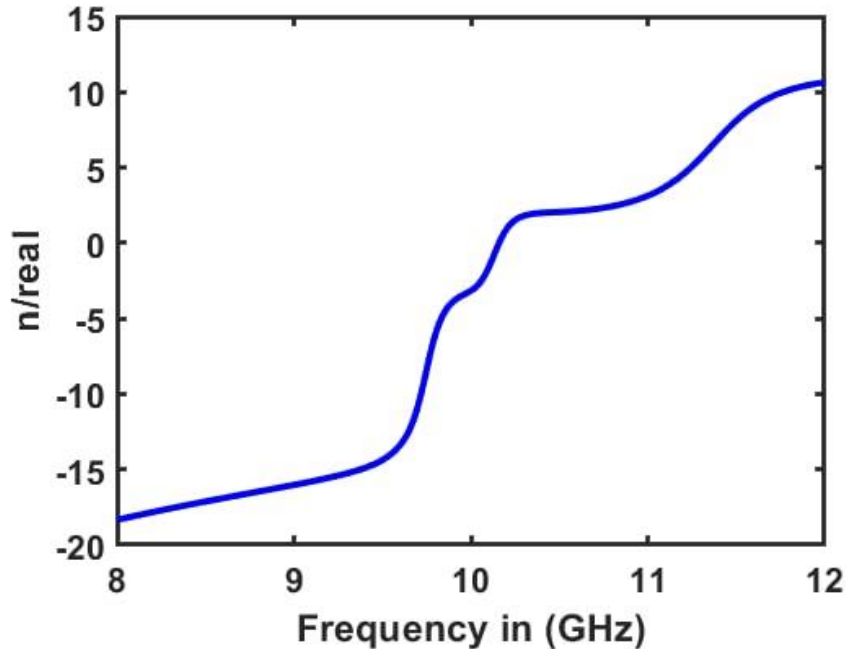


Figure 4.5: the negative refractive index.

4.2.5 The Current Distribution

Thus far, only the results have been shown in the thesis. Here, Fig.4.6 illustrates where the effective parts of the absorber are located. The current distribution is plotted at the resonance frequency of 10.14GHz. The red colour denotes the highest power absorbing parts, the green is the medium, and the blue is the lowest. As can be seen, the right and left edges confine the most power, whereas the lowest concentrates in a center of the unit cell.

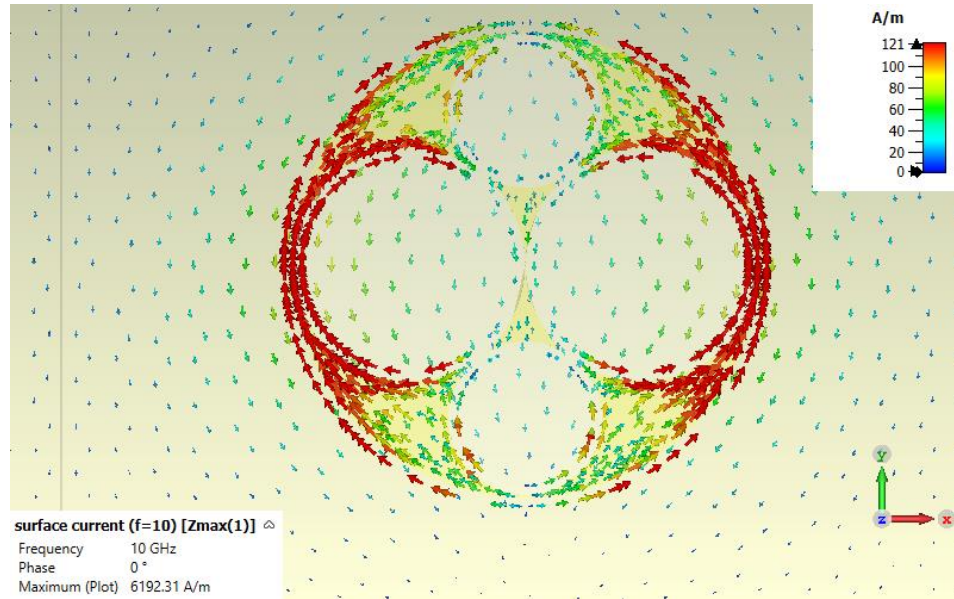
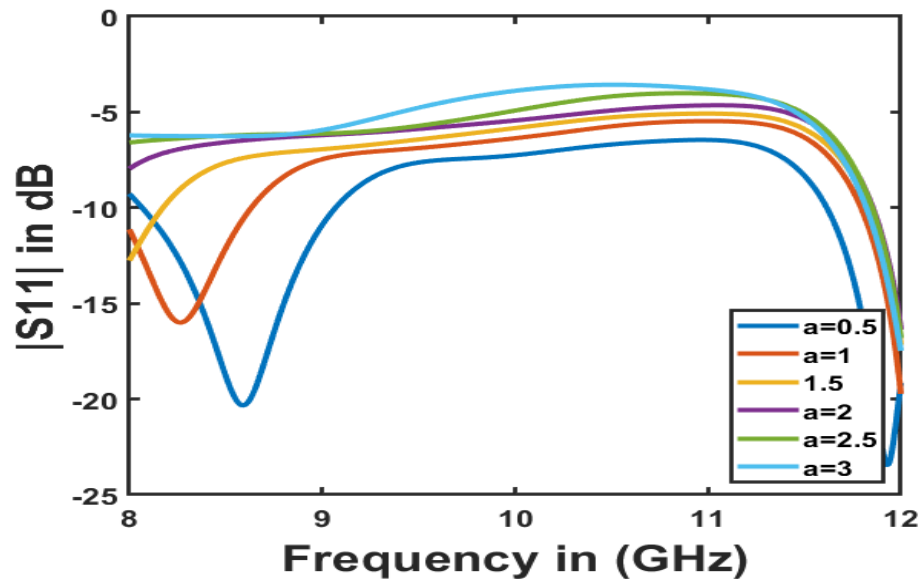


Figure 4.6: current distribution at the resonance frequency.

4.3 Study of the 3rd-iteration Modified Apollonian Gasket Unit Cell Metasurface of the Absorber (II)

The absorber here is developed relying on the nature of the fractal iteration. The iteration of the Modified Apollonian Gasket Unit Cell is started from the 0th iteration and is ended at the 3rd iteration. However, no big observable difference is in their results, so the results of the 3rd- iteration are only plotted for the sake of simplicity. The design setting in CST such as the dimensions, substrate type, boundary condition, and frequency analysis was done in Chapter 3. Only the results will be investigated here. Moreover, the design was tuned several times to obtain the optimum results. The process of absorption will not be repeated here because it is similar to the previous design, the last section.

Fig.4.7 shows the S_{11} for a range of substrate thicknesses (0.5mm-3mm with a step of 0.5mm). As can be seen, the structure resonates above the 8GHz with the best result obtained when the $h=3\text{mm}$ ($S_{11} < -20\text{dB}$). With this h , the absorber receives more than 99% of the incident power. This will be a good observation that the design will offer good performance. Moreover, the structure can absorb the power for a wide range of frequencies; see the figure (the S_{11} is about -10dB for $h=3\text{mm}$). For other thicknesses, the absorber still works almost fine. The proposed third iteration Apollonian Gasket fractal absorber exhibits benefits like dual-band at 8.6 GHz and 12 GHz with a broad range of absorption for x-band radar applications. This absorber has bandwidths for return loss -10 dB ranging from 8.1 GHz to 9.1 GHz for the lower band and 11.5 GHz to 12.5 GHz for the upper band. The absorber exhibits dual-band resonant frequency behaviour. This qualifies the suggested absorber for radar X-band applications.

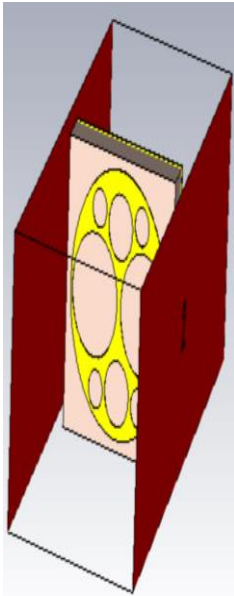


(A)

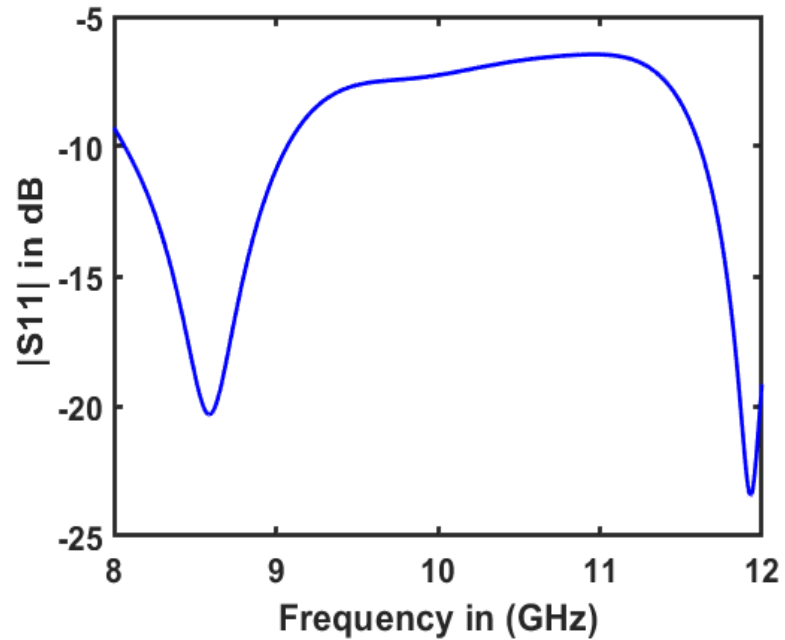
Figure 4.7: S_{11} vs the substrate thickness for the third iteration modified apollonian gasket unit cell metasurface of the absorber.

4.3.1 Extracting S-Parameters, ϵ , and μ of the 3rd-Iteration Modified Apollonian Gasket Metasurface Unit Cell of the Absorber

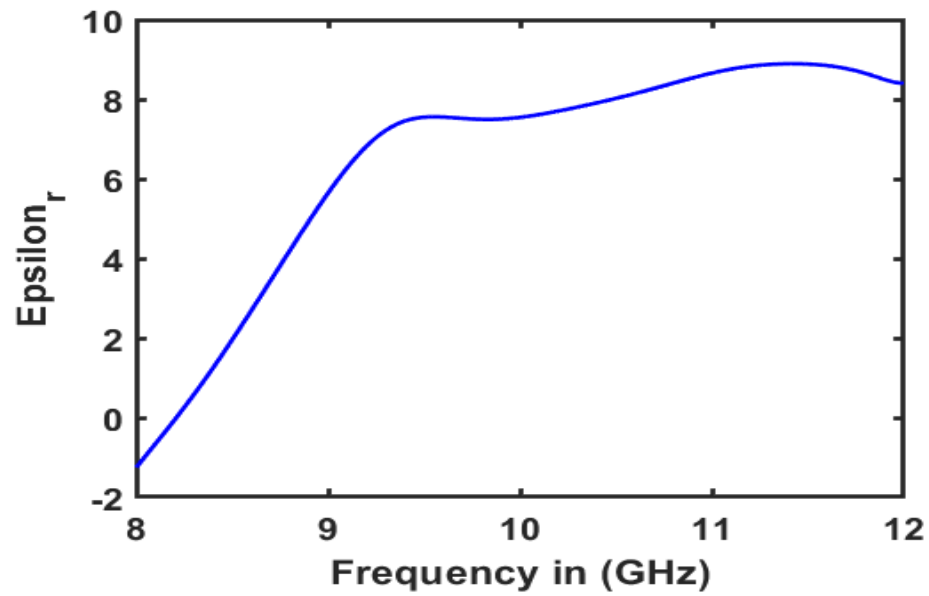
Having discussed the influence of the substrate thickness on the S11, the substrate is chosen as 3mm because it provides the best results. The results, in Fig.4.8, show that the proposed design can offer a very wide response extending from 8GHz to 12GHz. Also, the design resonates at the 8.55GHz and 12GHz with S11 of -20dB and -23.5dB, respectively. The constitution parameters of the proposed absorber are also plotted in Fig.4.8. The evidence is clear when observing them, and they are functions with frequency.



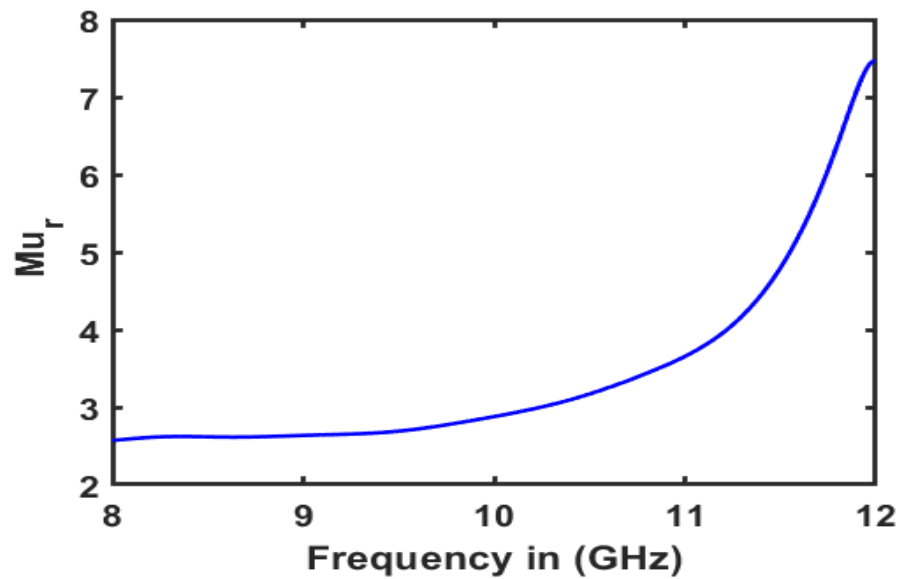
(A)



(B)



(C)



(D)

Figure 4.8: (A) the 3rd-iteration of Modified Apollonian Gasket metasurface unit cell (B) S11- parameter (C) permittivity (D) permeability

4.3.2 Extracting Absorption Coefficient from S-Parameters

Fig. 4.9 illustrates the results where maximum absorptivity for dual-band 3rd iteration metamaterial Apollonian Gasket is at 8.6GHz and 11.9GHz with an absorption coefficient of 98% and 99.5%, respectively.

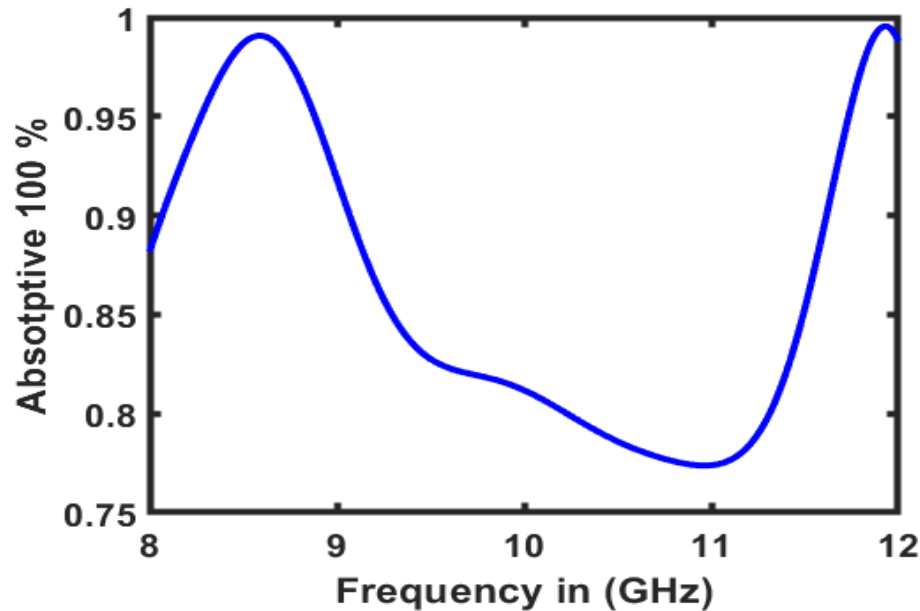


Figure 4.9: Absorption value of the 3rd iteration.

4.3.3 The Current Distribution

Fig. 4.10 shows the generation of current distributions of the absorber for the 3rd-iterations at a frequency of 11.9GHz. The result reveals that here again the vertical edges of the circular patch of the unit cell are responsible for confining the incident signals at the resonance frequency. Hence, when removing the circular slot parts from the centre of the patch, no apparent difference happens.

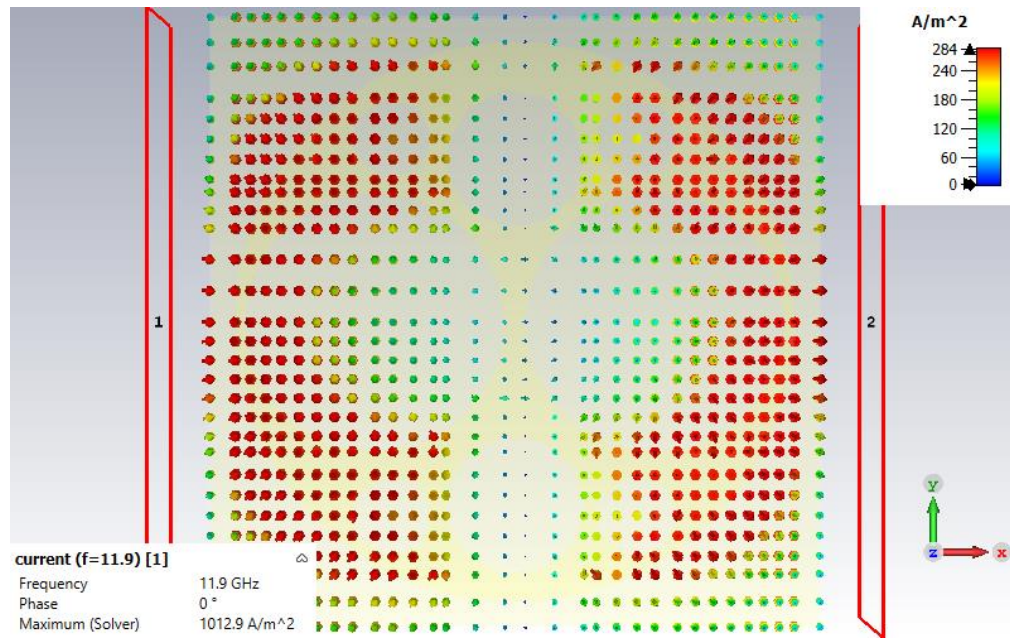


Figure 4.10: Current distributions of the 3rd iteration.

4.4 Parametric Study of the Sun Fractal Metasurface Absorber Unit Cell

In this section, another type of absorber is discussed and investigated. The structure was designed in Chapter 3, and the results will be introduced here. The h is altered to examine its effects on the S_{11} utilizing the CST. Fig.4.11 shows the results. The best value is chosen, leading to the highest absorption.

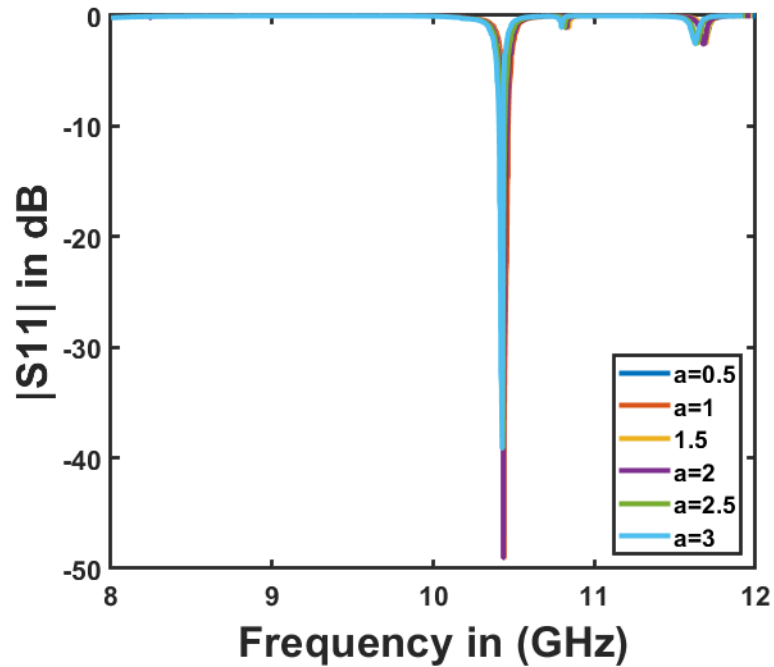
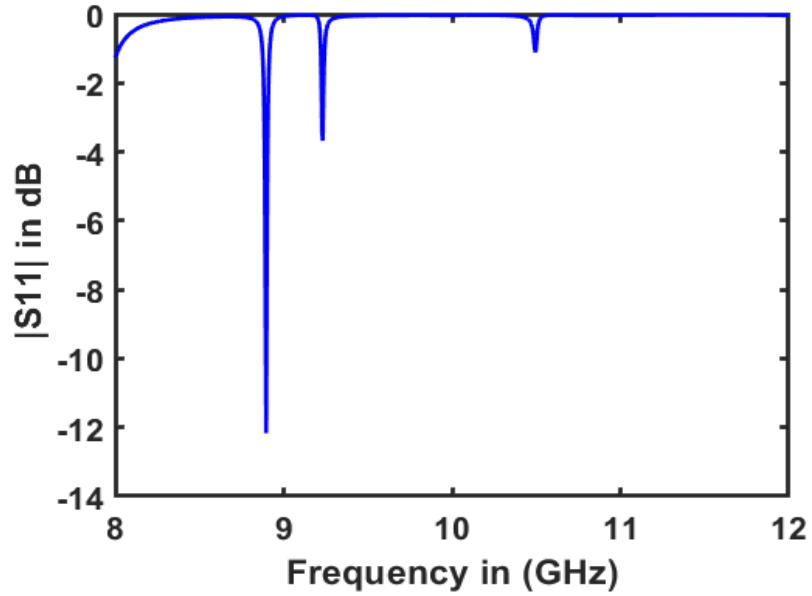


Figure 4.11: Parametric study of the Sun fractal metasurface absorber unit cell.

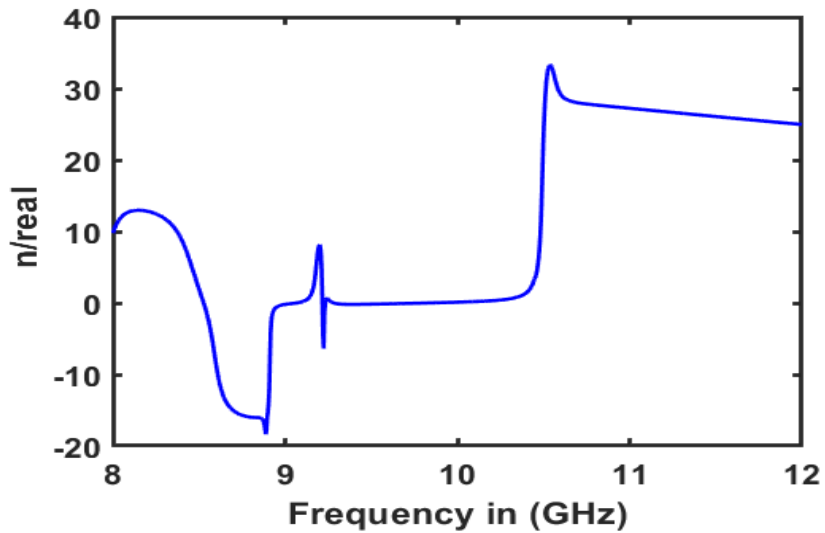
4.4.1 Extracting S-Parameter of the Sun Fractal Metasurface Absorber Unit Cell

The S_{11} is plotted in Fig.4.12, and it has several resonances (e.g., 8.1GHz, 8.9GHz, 9.3GHz, 10.5GHz, and 11GHz). The disadvantage here is the design has very narrow responses. However, it may be useful for some applications to avoid interference with other systems. Not all the resonances have good matching (i.e., $S_{11} < -10\text{dB}$), but they can be improved if the tuning is carried out carefully. The bandwidth of 1dB is larger than the bandwidth of -10dB. Also, Fig.4.12 displays the refractive index. As can be seen, the n has several curious places such as the negative, zero slope, and nonlinear trends. These places can be widely discussed in advanced electromagnetic

topics, when the n becomes zero at 8.9GHz, the absorptivity dominates the scene in the response.



(A)

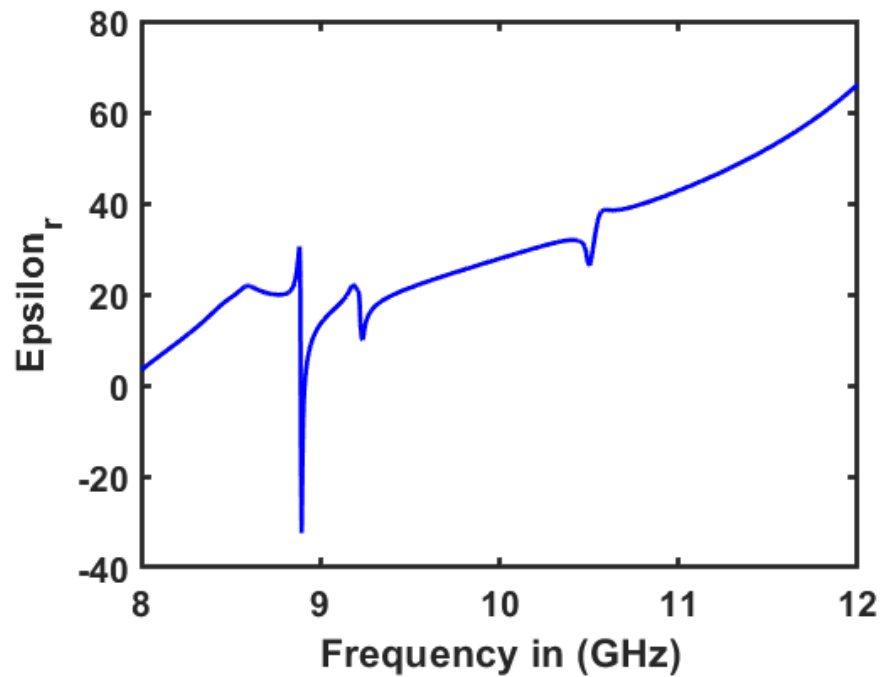


(B)

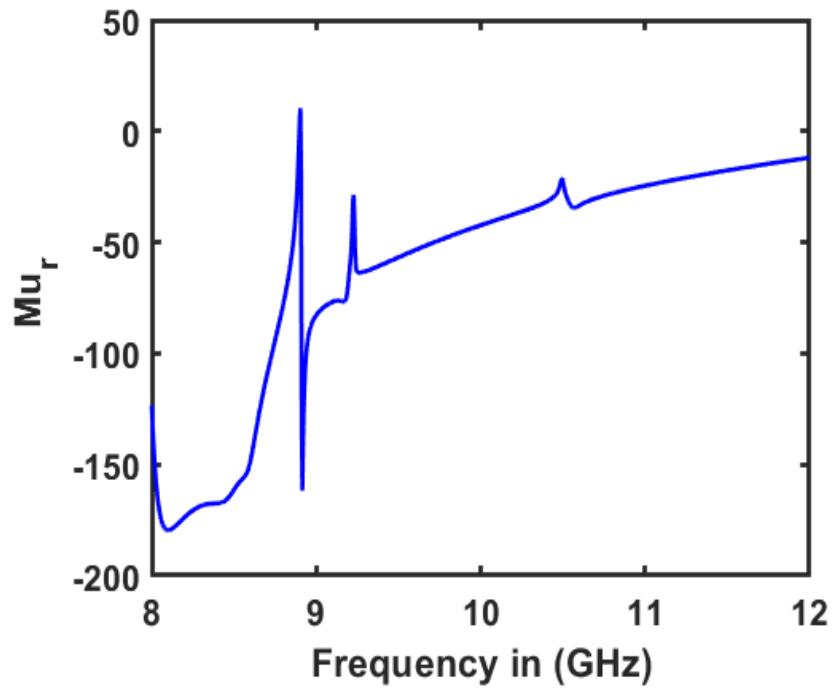
Figure 4.12: (A) S_{11} and (B) refractive index (n).

4.4.2 Extracting Permeability and Permittivity from S-Parameter

The variable permittivity and permeability govern the reflection index and can make it close to zero. Thus the power will be confined inside the absorber instead of reflecting or transmitting it. Both parameters have negative values at some frequency bands, leading to a negative refractive index, see Fig.4.13.



(A)



(B)

Figure 4.13: (A) permittivity (B) permeability values.

4.4.3 Extracting Absorption Coefficient from S-Parameters

Fig. 4.14 shows that the absorber has almost five peaks located at different frequencies. The best value is located at a resonant frequency of 8.9GHz.

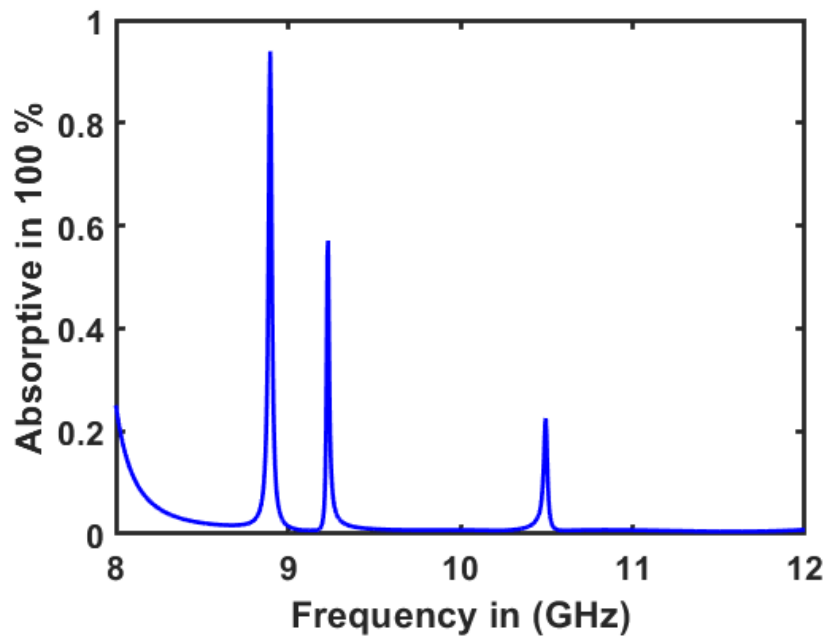


Figure 4.14: Absorption coefficient of the fractal sun unit cell.

4.4.4 Current Distributions

Fig. 4.15 shows the generation of current distributions for the absorber at a frequency of 8.9GHz. The current density is observed in the absorber's outer ring, indicating the maximum absorption with the red arrows.

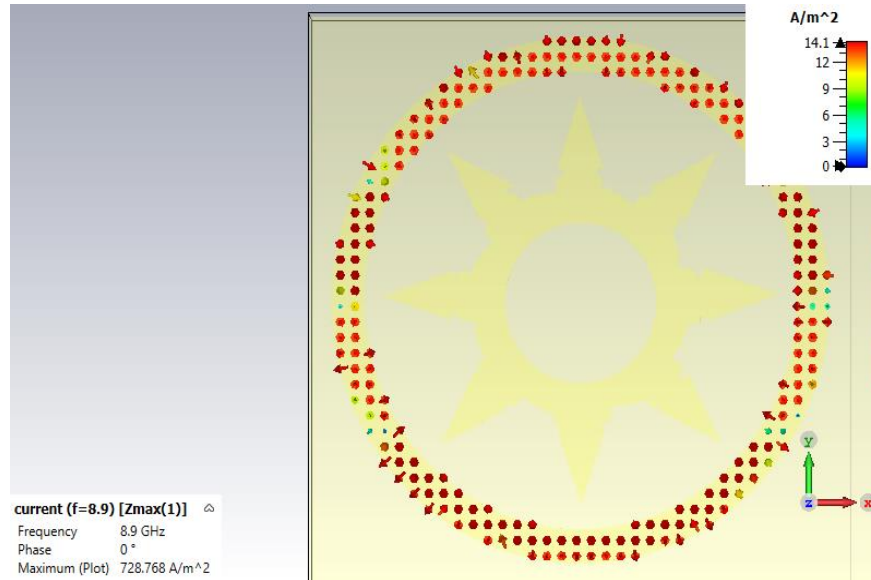


Figure 4.15: current distribution for the sun fractal unit cell.

4.5 Comparison and Discussion of the Results

Table 4.1 provides a summary of all previous discussions and compares the related references and this work in terms of absorber size, resonance frequency, absorber bandwidth, and absorption ratio. The comparison shows that the first design (Apollonian Gasket Fractal) has a very high absorption rate reaches 99.7% at the resonant frequency of 10.14GHz compared to [6] and enhancement in the bandwidth which is equal to 1.5GHz and with a size smaller than [6]. Moreover, the fourth design (Sun-Modified Fractal) satisfies an enhancement in the bandwidth with a very high absorption rate reaching 95.5% with the enhancement in the bandwidth of 1.5GHz, and with a smaller size compared to [9]. All details of absorption of the proposed absorbers are plotted in Fig.4.16.

As demonstrated earlier, the process of power trapping (i.e., power absorbing process) is determined when the absorber offers negative permittivity and permeability. Also, the reflection index will be changed from negative to positive, passing through zero. At the zero value ($n=0$), the surface will confine the power instead of reflecting or transmitting it ($A=1$). The power confinement is very clear when we sketch the induced current distribution over the absorber surfaces. The weak and strong locations of current distributions show where the power is trapped inside the structures. Moreover, varying the permittivity and permeability changes the impedance of the absorber. If the impedance becomes equal to the free-space impedance, the impedance matching occurs (i.e., no reflection and full absorption). Practically, all parameters mentioned above function with frequency, thereby offering good performances at specific bands of frequencies. The S_{11} and Absorption plots are the criteria to show the system performance. For example, when S_{11} decreases more than -10dB , the A will become close to unity. Also, the n will be zero and the impedance of the absorber will be equal to the free-space impedance.

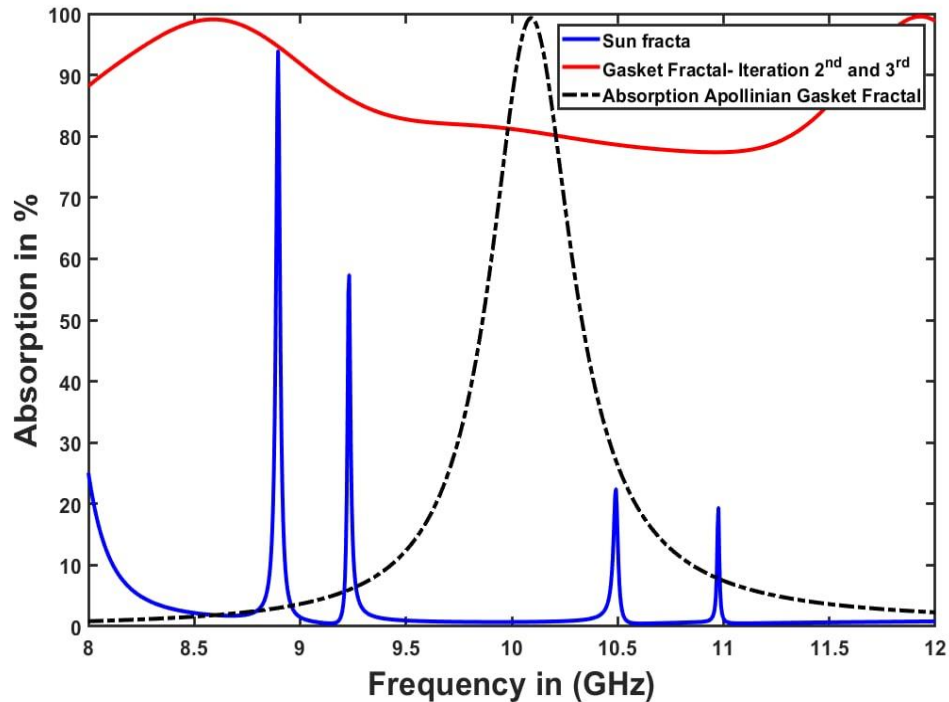


Figure 4.16: Comparison of the absorption coefficient of all proposed absorbers.

All details of S_{11} of the proposed absorbers are plotted in Fig. 4.17. As demonstrated earlier, the process of power trapping (i.e., power absorbing process) is determined when the absorber offers negative permittivity and permeability. Also, the reflection index will be changed from negative to positive, passing through zero. At the zero value ($n=0$), the surface will confine the power instead of reflecting or transmitting it ($A=1$). The power confinement is very clear when we sketch the induced current distribution over the absorber surfaces. The weak and strong locations of current distributions show where the power is trapped inside the structures. Moreover, varying the permittivity and permeability changes the impedance of the absorber. If the impedance becomes equal to the free-space impedance, the impedance matching occurs

(i.e., no reflection and full absorption). Practically, all parameters mentioned above function with frequency, thereby offering good performances at specific bands of frequencies. The S11 and Absorption plots are the standards to show the system performance. For example, when S11 decreases more than -10dB, the A will become close to unity. Also, the n will be zero and the impedance of the absorber will be equal to the free-space impedance.

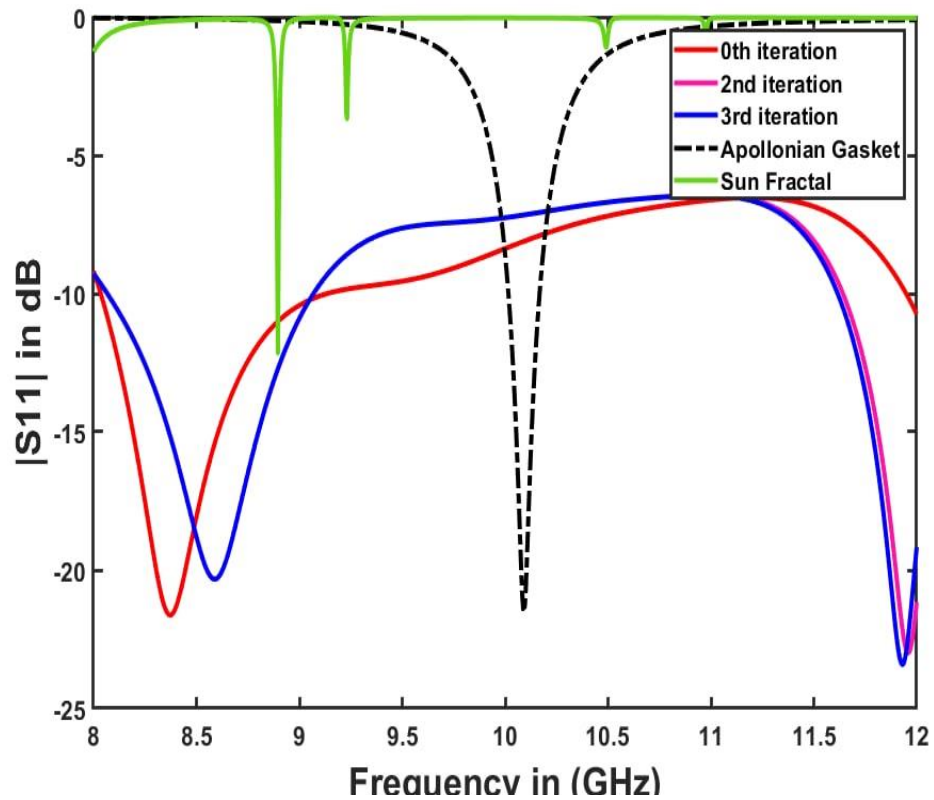


Figure 4.17: Comparison of the S11 coefficient of all proposed absorbers.

TABLE 4.1 Comparisons among the three designs of the proposed absorbers
and with other related works

Ref.	Design name	Dimensions (mm)	S11 (dB)	Frequency (GHz)	Bandwidth (GHz)	Absorption (%)
[4]-[12]	Ultra-thin-Fractal Shaped Metamaterial Absorber	a = 15 b = 9 h = 1.7	-	10.5	1	99.1
[6]-[14]	Bandwidth-enhanced-Metamaterial Absorber	a = 11 l1 = 10.8 h = 1.6	-	8.7 & 9.93	1.73	98.14 & 99.22
[9]-[17]	Simulation Design of Dual Band Metamaterial Absorber	a = 37 b = 37 h = 1.6	-20	2.3 & 7	1.3	99.5
This work	First Design (Apollonian Gasket Fractal)	a = 10 d1 = 2.35 h = 1	-21	10.14	1.5	99.7
	Second Design (Modification of Apollonian Gasket- 3 rd iteration)	r ₃ = 0.41 h = 0.5	-20 & -23	8.6 & 11.9	1.1 & 1.2	99 & 99.5
	Third Design (Sun fractal)	a = 25 b = 25 h = 1	-12	8.9	1.5	95.5

CHAPTER FIVE**CONCLUSION AND FUTURE WORK****5.1 Introduction**

This chapter introduces the main points presented in this thesis and future works.

5.2 Conclusion

Three different types absorbers were designed, simulated, and parametrically studied. The first thing was the study of unit cells. Each type of unit cell is affected to extract the actual results: the reflection coefficient S_{11} , the absorption coefficient A , and the current distributions on the structure at the resonance frequencies. All arrangements could absorb the power ratio close to unity (i.e., more than 95%). This is the critical advantage of our proposed designs. For each unit cell, the periodic boundary condition was applied to the side walls of the waveguide to mimic the infinite array of unit cells the normal boundary condition aided in accelerating the simulation process. The first type of SAM could absorb the incident power up to 99.7% at 10.14GHz, which was very close to the unity. Also, the unit cell matches the free space impedance very well. Secondly, the other type of SAM consisted of fractal shapes that were iterated until the fourth stage in uniform and gradient ways. It was able to absorb the power until 97% at 9.5GHz. Its S_{11} was very good at that frequency band.

Moreover, all other unit cells were arranged in array forms to create the SAM planes. The parametric sweep tool in the CST was used to study each element of the absorber designs to get the best performance. Finally, the first absorber was the most effective among the four absorbers in absorption coefficient, which was about 99.7% with negative permeability and permeability.

5.3 Future Work Recommendations

The following points are suggested for further investigation depending on the results of this thesis:

- 1.** Investigating the Material change effects on the absorption coefficient.
- 2.** Building multi-layer absorbers to operate at the diffident band to cover many applications.
- 3.** Integrating electronic switches to reconfigure the responses.
- 4.** Integrating rectifiers to make the absorbers operate as energy harvesters.
- 5.** Fabricating and testing the presented SAMs addressed in this thesis.

REFERENCES

- [1] Seo, I. S., Chin, W. S., & Lee, D. G. (2004). Characterization of electromagnetic properties of polymeric composite materials with free space method. *Composite Structures*, 66(1–4), 533–542.
- [2] Moradi, E., Björninen, T., Ukkonen, L., & Rahmat. S.Y. (2012). Characterization of Embroidered Dipole-type”, *RFID-Technologies and Applications (RFID-TA)*, IEEE International Conference, 5-7 Nov.
- [3] C.M. Roberts. (2006). *Radio frequency identification (RFID)*. Computer and Security.
- [4] Vinoy, K. J., & Jha, R. M. (1995). *Trends in radar absorbing materials technology* (Vol. 20).
- [5] Knott, E.F., Shaeffer, J.F., & Tuley, M.T. (1988). *Radar Cross Section*, Artech House, Norwood, Massachusetts, pp.198 - 218.
- [6] Shimizu, Y., & Suetake, K. (1968). Minimum-Thickness Design of Broad-Band Absorbing Wall, *Trans. I.E.C.E., Japan*, Vol. 51B, No.3, pp.57 – 63.
- [7] Lagar'kov, A. N., Kisel', V. N., & Semenenko, V. N. (2012). Radar absorbers based on metamaterials. *Journal of Communications Technology and Electronics*, 57(10), 1122–1129.
- [8] Skolnik, M. (1962). *Radar Handbook*, McGraw-Hill, New York, pp.11.43 - 11.56.
- [9] Nong, FY, Zhi,C.Y., Ming,D.Y., & Zhou,G.R.(2012). Absorbing Performance of Ultrathin Wide-Band Planar Metamaterial Absorber.*IEEE*, 978-1-4673-1800-6.
- [10] Cheng, Y. Z., Nie, Y., & Gong, R. Z. (2013). Design of a wide-band metamaterial absorber based on fractal frequency selective surface and resistive films. *Physica Scripta*, 88(4). <https://doi.org/10.1088/0031-8949/88/04/045703>.

- [11] Munaga, P., Ghosh, S., Bhattacharyya, S., & Srivastava, K. V. (2016). A fractal-based compact broadband polarization insensitive metamaterial absorber using lumped resistors. *Microwave and Optical Technology Letters*, 58(2), 343–347.
- [12] Bhattacharyya, S., Ghosh, S., Bhattacharya, A., Chaurasiya, D., & Vaibhav, K. (2015). An Ultra-thin Polarization Independent Compact Fractal Shaped Metamaterial Absorber. *IEEE*, 978-1-4673-9536-6.
- [13] Dingwang, Y., Liu, P., & Dong, Y. (2016). A novel Miniaturized Metamaterial absorber Based on the modified Minkowski fractal structure. *IEEE*, 978-1-4673-9494-9.
- [14] Fan, S. & Song, Y. (2018). Bandwidth-enhanced polarization-insensitive metamaterial absorber based on fractal structures. *journal of applied physics* 123, 085110.
- [15] Venneri, F., Costanzo, S., & Borgia, A. (2019). A dual-band compact metamaterial absorber with fractal geometry. *Electronics (Switzerland)*, 8(8).
- [16] Chen, T., Li, S. J., Cao, X. Y., Gao, J., & Guo, Z. X. (2019). Ultra-wideband and polarization-insensitive fractal perfect metamaterial absorber based on a three-dimensional fractal tree microstructure with multi-modes. *Applied Physics A: Materials Science and Processing*, 125(4).
- [17] Ling, K., Yoo, M., & Lim, S. (2015). Frequency Tunable Metamaterial Absorber Using Hygroscopicity of Nature Cork. *IEEE Antennas and Wireless Propagation Letters*, 14, 1598–1601.
- [18] Dileep, A., Abhilash, P. V., Joy, V., Singh, H., Nair, R. U. (2020). Metamaterial Absorber based on Minkowski Fractal Patch for Stealth Applications”, *IEEE Xplore*, september.
- [19] Li, Q., Dong, J., Li, T., & Cao, X. (2020). Broadband Fractal Tree Metamaterial Absorber for P and L Bands Applications. *IEEE*, 978-1-7281-9045-7.
- [20] BILAL, R. M. H., BAQIR, M. A., Choudhury, P. K., Karaaslan, M., Ali, M. M. O. Altintas, A. A., Rahim, E., & Sabah, C. (2021). Wideband Microwave Absorber

Comprising Metallic Split-Ring Resonators Surrounded with E-Shaped Fractal Metamaterial”, IEEE ACCESS, 10.1109.

[21] Agbaeze Eteng, A. (2021). Design of a Compact Fractal Unit Cell Absorber for the 2.45 GHz Band. *International Journal of Wireless and Microwave Technologies*, 11(1), 15–21.

[22] Bilal, R.M.H., & Naveed, M.A. (2021). A comment: a set square design metamaterial absorber for X-band applications. *Journal of Electromagnetic Waves and Applications*, 35(10):1-5.

[23] Yaman MD. (2015). Thin film coating of glass fabrics for radar absorbing composites. Unpublished master’s thesis. İzmir, Turkey: İzmir Institute of Technology.

[24] Micheli, D., Vricella, A., Pastore, R., & Marchetti, M. (2014). Synthesis and electromagnetic characterization of frequency selective radar absorbing materials using carbon nanopowders. *Carbon*, 77, 756–774.

[25] Silveira Pinho, M., Luisa Gregori, M., elia Reis Nunes, R. C., & Guenther Soares, B. (n.d.). Performance of radar absorbing materials by waveguide measurements for X- and Ku-band frequencies.

[26] Fan, Z., Luo, G., Zhang, Z., Zhou, L., & Wei, F. (2006). Electromagnetic and microwave absorbing properties of multi-walled carbon nanotubes/polymer composites. *Materials Science and Engineering B: Solid-State Materials for Advanced Technology*, 132(1–2), 85–89.

[27] Wu, M., He, H., Zhao, Z., & Yao, X. (2000). Electromagnetic and microwave absorbing properties of iron fibre-epoxy resin composites. In *J. Phys. D: Appl. Phys* (Vol. 33).

[28] Park, K. Y., Lee, S. E., Kim, C. G., & Han, J. H. (2006). Fabrication and electromagnetic characteristics of electromagnetic wave absorbing sandwich structures. *Composites Science and Technology*, 66(3–4), 576–584.

- [29] Peng, Z. H., Cao, M. S., Yuan, J., & Xiao, G. (2004). Strong fluctuation theory for effective electromagnetic parameters of fiber fabric radar absorbing materials. *Materials and Design*, 25(5), 379–384.
- [30] Oh, J. H., Oh, K. S., Kim, C. G., & Hong, C. S. (2004). Design of radar absorbing structures using glass/epoxy composite containing carbon black in X-band frequency ranges. *Composites Part B: Engineering*, 35(1), 49–56.
- [31] Marqués, R., Martín, F., & Sorolla, M. (2011). *Metamaterials with negative parameters: theory, design, and microwave application*. vol. 183. John Wiley & Sons.
- [32] Solymar, L., & Shamonina, E. (2009). *Waves in metamaterials*. Oxford University Press.
- [33] Veselago, V. G. (1967). Electrodynamics of substances with simultaneously negative values ϵ and μ . *Usp. Fiz. Nauk*, vol. 92, p. 517.
- [34] Pendry, J. B., Holden, A. J., Robbins, D. J., & Stewart, W. J. (1998). Low frequency plasmons in thin-wire structures. In *J. Phys.: Condens. Matter* (Vol. 10).
- [35] Pendry, J. B., Holden, A. J., Robbins, D. J., & Stewart, W. J. (1999). Magnetism from Conductors and Enhanced Nonlinear Phenomena. In *IEEE TRANSACTIONS ON MICROWAVE THEORY AND TECHNIQUES* (Vol. 47, Issue 11).
- [36] Smith, D. R., Padilla, W. J., Vier, D. C., Nemat-Nasser, S. C., & Schultz, S. (2000). Composite Medium with Simultaneously Negative Permeability and Permittivity.
- [37] Tretyakov, S., Barois, P., Scharf, T., Kruglay, V., & Bergmair, I. (2010). *Nanostructured Metamaterials*.
- [38] Chen, X., Grzegorzczak, T. M., Wu, B. I., Pacheco, J., & Kong, J. A. (2004). Robust method to retrieve the constitutive effective parameters of metamaterials. *Physical Review E - Statistical Physics, Plasmas, Fluids, and Related Interdisciplinary Topics*, 70(1), 7.

- [39] Engheta, N., & Ziolkowski, R. W. (2006). *Metamaterials: physics and engineering explorations*. John Wiley & Sons.
- [40] Pendry, J. B. (2000). Negative refraction makes a perfect lens., *Phys. Rev. Lett.*, vol. 85, no. 18, p. 3966.
- [41] Ramakrishna, S. A., & Grzegorzczak, T. M. (2008). *Physics and applications of negative refractive index materials*. CRC press.
- [42] Ziolkowski, R. W., & Heyman, E. (2001). Wave propagation in media having negative permittivity and permeability. *Physical Review E - Statistical Physics, Plasmas, Fluids, and Related Interdisciplinary Topics*, 64(5), 15.
- [43] Smith, D. R., Padilla, W. J., Vier, D. C., Nemat-Nasser, S. C., & Schultz, S. (2000). Composite Medium with Simultaneously Negative Permeability and Permittivity.
- [44] Kenneth, F. (2003). *Fractal Geometry: Mathematical Foundations and Application*. Second Edition, John Wiley & Sons, Ltd.
- [45] Fawwaz, J. J., & Zahraa F. M. (2009). Comparison of the Radiation Characteristics of Triangular and Quadratic Koch Fractal Dipole Wire Antennas. *Iraqi Society for Alternative and Renewable Energy Sources and Techniques* 18 (ISAREST).
- [46] Engheta, N., & Richard W. Z. (2006). *Metamaterials: physics and engineering explorations*. 13 978-0-471-76102-0.
- [47] Caloz, Christophe; Itoh, T. (2005). *Electromagnetic metamaterials: transmission line theory and microwave applications*. John Wiley & Sons, 0-471-66985-7.
- [48] John, W., & sons. (2005). *Antenna Theory Analysis and Design*”, third edition, 0-471-66782-X.
- [49] Iyampalam, P., & Ganesan, I. (2020). Low profile antenna based on a fractal shaped metasurface for public safety applications. *International Journal of RF and Microwave Computer-Aided Engineering*, 30(2).

[50] Numan, A. B., & Sharawi, M. S. (2013). Extraction of Material Parameters for Metamaterials Using a Full-Wave Simulator. In *IEEE Antennas and Propagation Magazine* (Vol. 55, Issue 5).

[51] Tamim, A. M., Faruque, M. R. I., Alam, M. J., Islam, S. S., & Islam, M. T. (2019). Split ring resonator loaded horizontally inverse double L-shaped metamaterial for C-, X- and Ku -Band Microwave applications. *Results in Physics*, 12, 2112–2122.

[52] Simovski, C. R., Pavel A. B., & Saling H. (2003). Backward wave region and negative material parameters of a structure formed by lattices of wires and split-ring resonators. *IEEE Transactions on Antennas and Propagation* 51, 2582-2591.

[53] Chen, X., Grzegorzczak, T. M., Wu, B. I., Pacheco, J., & Kong, J. A. (2004). Robust method to retrieve the constitutive effective parameters of metamaterials. *Physical Review E - Statistical Physics, Plasmas, Fluids, and Related Interdisciplinary Topics*, 70(1), 7.

[54] Balanis, C.A.(2016). *ANTENNA THEORY ANALYSIS AND DESIGN*. Courtesy NASA/JPL-Caltech.

[55] Zakariyya, S. O. (2015). Modeling of Miniaturized, Multiband and Ultra-Wideband Fractal antenna. Master's Thesis. Eastern Mediterranean University (EMU)-Doğu Akdeniz Üniversitesi (DAÜ).

[56] Borah, D., Bhattacharyya, N. S. (2017). Design, fabrication and characterization of flexible and ultrathin microwave metamaterial absorber. *IEEE International Conference on Innovations in Electronics, Signal Processing and Communication (IESC)*.

[57] Heath, T.L. (1961). Apollonius of Perga. *Treatise on Conic Sections*

[58] Anooz, R. S. A., Hatem, G. M., Hasnawi, I. H. Y., & Nemah, M. N. (2021). Design Apollonian Gasket Antenna for Millimeter-Wave Applications. *IOP Conference Series: Materials Science and Engineering*, 1094(1), 012038.

[59] Smith, D. R., Vier, D. C., Koschny, T., & Soukoulis, C. M. (2005).
Electromagnetic parameter retrieval from inhomogeneous metamaterials. *Physical Review E - Statistical, Nonlinear, and Soft Matter Physics*, 71(3).

Appendix

Publications Papers

Indexed by Clarivate analytics and Scopus (Q3)

NeuroQuantology | July 2022 | Volume 20 | Issue 8 | Page 8758-8764 | doi:10.14704/nq.2022.20.8.NQ44898
Wassan Hassan Yaseen et al/ A Review on Metamaterial Absorber based on Fractal geometry



A Review on Metamaterial Absorber based on Fractal geometry

Wassan Hassan Yaseen 1* Ghufran M. Hatem 1* Abdulkadhum J.Yasiri1*

1Department of communication engineering Najaf Technical College, Al-Furat Al-Awsat Technical University (ATU) , Al-Najaf Al-Ashraf, Iraq
Email: Wassan.Yaseen.Me.etch @ student.atu.edu.iq

Abstract—

Defense modern communication systems have recently required more complicated design and operating features. Smaller devices can be combined for different communication systems and implemented in one user's device board. Furthermore, the cost of structure production should be kept to a minimum. The absorber of these devices should be compact, light, operate in various frequency bands, and/or be broadband to meet part of that request. There are numerous research strategies for achieving this goal, one of which is the use of fractal geometries for absorber element shape. Many fractal forms have been proposed for such applications in recent years, and the constructed antennas have greatly improved. In addition of using fractal the use of Metamaterial (MMT) with negative permittivity and permeability values to design absorber and get a high absorption rate is recently investigated. The advantages of employing fractal-based MMT arrangement to create radio and microwave absorbers were discovered in this paper.

This paper provides a good review of the different fractal geometry types that are used to design MMT absorbers. This study's objective is to showcase the most recent discoveries and academic studies related to the subjects mentioned above.

Keywords:Metamaterial, fractal geometry, absorber, self-similarity, space filling.

DOI Number:10.14704/nq.2022.20.8.NQ44898

NeuroQuantology 2022; 20(8): 8758-8764

8758

INTRODUCTION

Engineers and scientists working in this field have noted the rapid growth of communication technology over the years. People have been encouraged to best their life goodness by utilizing technological breakthroughs. In the electronics turf, microwave absorber is used to reduce the quantum of electromagnetic wave upset Electromagnetic interference (EMI) [1–2]. However, that once coated material is enveloped by microwave absorber, the

eISSN1303-5150

impact of EMI can be avoided. This behavior is depicted in Figure 1. Defense (military) [3, 4]. As shown in Figure 2, this reflector is used to coat or spray military facilities and equipment such as "strike aircraft", "warships (war ships), and "military uniforms", especially personnel in the guard front. A radar system's transmitter sends out microwave in all directions all the time. If this wave hits something, the signal is reflected and transmitted to the receiver. This relative

www.neuroquantology.com



Apollonian Gasket Fractal Based Metamaterial Absorber for X-Band Radar Applications

Wassan Hassan Yaseen^{*1}, Ghufan M. Hatem² & Abdulkadhum J. Yasiri³

^{*1,2&3}Department of Communication Engineering Najaf Technical College, Al-Furat Al-Awsat Technical University (ATU), Al-Najaf Al-Ashraf, Iraq

ABSTRACT

In recent years, there are a lot of attentiveness in the study of absorbers, because of their wide-ranging applications especially in military. As a result of their compactness throughout all frequency ranges, metamaterial-based absorbers are also discovered to be of significant interest. The metamaterial (MM) tasks as a left-hand material with negative permittivity and permeability, which results in a low refractive index. Because of their properties it used in many applications, one of its applications is to design a radar absorber. In this paper, the unit cell of the proposed structure is based on Apollonian second iteration gasket fractal geometry to introduce an X-band (8-12_GHz) metamaterial absorber for radar military applications. It consists of a substrate layer as FR-4 layer of a thickness 1mm and PEC circle fractal loaded on it. There is air gap exist between the absorber slot. The results show that The structure has peak absorption 99.7 % with 2GHz bandwidth. Due to changes in the equivalent relative permeability and permittivity of the structure the overall absorber performance has been enhanced.

Keywords: Metamaterial, Apollonian gasket, Absorber, radar.

I. INTRODUCTION

In the last years prior to the discovery of metamaterials (MTM) and the innovative attributes that they contain that are not found in nature, scientific study was focused on developing the properties of materials utilized to offer unique specifications in accordance with their practical utilization. Because of these qualities, there is no widely accepted definition of a metamaterial, but all descriptions that are widely accepted are of artificial materials that get their properties from their structure rather than their composition and may produce strange electromagnetic phenomena that are difficult for natural materials to produce [1]. Metamaterials have a wide range of technological uses, including perfect lenses [2], cloaking [3] and absorbers [4]. The structural component of a metamaterial is designed to exhibit an electric / magnetic response or resonance at a specific frequency. Metamaterials are created using various split rings or periodic structures made of highly conductive metals like gold, silver, or copper [5].

Engineers and scientists working in this field have noted the rapid growth of communication technology over the years. People have been encouraged to best their life goodness by utilizing technological breakthroughs. In the electronics turf, microwave absorber is used to reduce the quantum of electromagnetic wave upset Electromagnetic interference (EMI) [6-7]. However, that once coated material is enveloped by microwave absorber, the impact of EMI can be avoided. This behavior is depicted in Figure 1. Defense (military) [8, 9]. As shown in Figure 2, this reflector is used to coat or spray military facilities and equipment such as "strike aircraft", "warships "(war ships), and "military uniforms", especially personnel in the guard front. A radar system's transmitter sends out microwave in all directions all the time. If this wave hits something, the signal is reflected and transmitted to the receiver. This relative contribution indicates the existence of a nearby item, that will be displayed during the radar scanner. Radar (radio detection and ranging) is a microwaves technique for detecting, measuring, and mapping things. Radar waves can detect the presence of targets [6]. The radar calculates the range between the target and the radar. The ranges measured by the time delay between the transmitted and reflected signal to the radar. The radar can reveal the presence of these objects because the target may reflect electromagnetic radiation. The radar, on the other hand, will be unable to detect the item if it does not reflect radar signals [7]. This tendency is then used for the benefit of a certain defensive system. Microwave absorbent materials are widely used, and it is well understood that they can lower the power of electromagnetic waves [8]. These microwave absorptive materials can be utilized outside or inside to reduce or eliminate reflections or transmissions from specified objects [9]. This microwave absorbent can also be utilized to create an environment that is devoid of reflections or anechoic. Many researchers have used a number of novel techniques to design a microwave absorber for many purposes [9].

الخلاصة

يعد امتصاص الإشارات الكهرومغناطيسية المنعكسة من الطائرات موضوعاً مهماً في التطبيقات العسكرية. يلعب تقليل كمية طاقة الأمواج المنعكسة دوراً حيوياً في تحديد موقع الطائرة في السماء. ستتعامل هذه الأطروحة مع هذه القضية من خلال تقديم مادة امتصاصية جديدة مركبة SAM. أنظمة SAM المقترحة قادرة على تقليل قوة الانعكاس بأكثر من 95٪، وسيوفر هذا التخفيض بديلاً جيداً للتطبيقات العسكرية والتجارية على حد سواء.

تم اقتراح ثلاث خلايا وحدة مختلفة على أساس الهندسة الكسورية. يتم ترتيب خلايا الوحدة المقترحة في طائرات لإنشاء المواد ذات اليد اليسرى (LHMs) أي (SAM) القادرة على حصر قوة الحادث بدلاً من إعادتها إلى حيث أنت لأن SAM لها سماحية ونفاذية سلبية في نطاقات محددة من الترددات التي تعمل على النطاق (8-12) X (جيجاهرتز). تم اعتماد الركييزة FR4 مع ثابت العزل 4.3 ، وسمك 1 مم ، وظل الخسارة 0.025 في جميع التصميمات والمحاكاة. تتم طباعة خلايا الوحدة المقترحة على الوجه العلوي النحاسي للركييزة.

الهندسة الكسورية Apollonian Gasket هي النوع الأول من خلايا الوحدة التي تمت محاكاتها. توجد فجوة هوائية بين فتحات الامتصاص. أظهرت النتائج أن الهيكل لديه أعلى نسبة امتصاص بنسبة 99.7٪ لوحظ عند 10 جيجاهرتز مع عرض نطاق 1.5 جيجاهرتز. نظراً للتغيرات في النفاذية النسبية والسماحية المكافئة للهيكل ، فقد تم تحسين أداء الامتصاص الكلي. يعتمد الهيكل المصمم الثاني على الهندسة الكسورية للشمس الحلقية المعدلة حيث يتم قطع خلية الوحدة من رقعة الامتصاص. أظهرت النتائج أن الهيكل يتمتع بأقصى امتصاص بنسبة 95.5٪ عند 8.9 جيجا هرتز مع عرض نطاق 1.3 جيجا هرتز. يُظهر كلا الماصين أنهما يمكنهما تحقيق امتصاص عالي في نطاقات تردد X مختلفة يمكن استخدامها في مجموعة متنوعة من تطبيقات الرادار العسكرية. تتم دراسة هياكل التصميم ومحاكاتها باستخدام حزمة CST لاستوديو الميكروويف. أخيراً، تقدم الأطروحة نوعاً آخر من أنظمة SAM ذات نسبة امتصاص عالية.



تصميم ومحاكاة جهاز امتصاص يعتمد على الهندسة الكسورية في تطبيقات X- باند

الرسالة

مقدمة الى قسم هندسة تقنيات الاتصالات كجزء من متطلبات نيل درجة الماجستير في هندسة

تقنيات الاتصالات

تقدمت بها

وسن حسن ياسين

إشراف

د. غفران مهدي حاتم

أ.د. عبد الكاظم الياسري

تشرين الاول / 2022



جمهورية العراق

وزارة التعليم العالي والبحث العلمي

جامعة الفرات الاوسط التقنية

الكلية التقنية الهندسية – نجف

تصميم ومحاكاة جهاز امتصاص يعتمد على الهندسة الكسورية

في تطبيقات X-باند

وسن حسن ياسين

ماجستير في هندسة تقنيات الاتصالات

2022